Neuron

Article

# Neural circuit underlying individual differences in visual escape habituation

## Graphical abstract

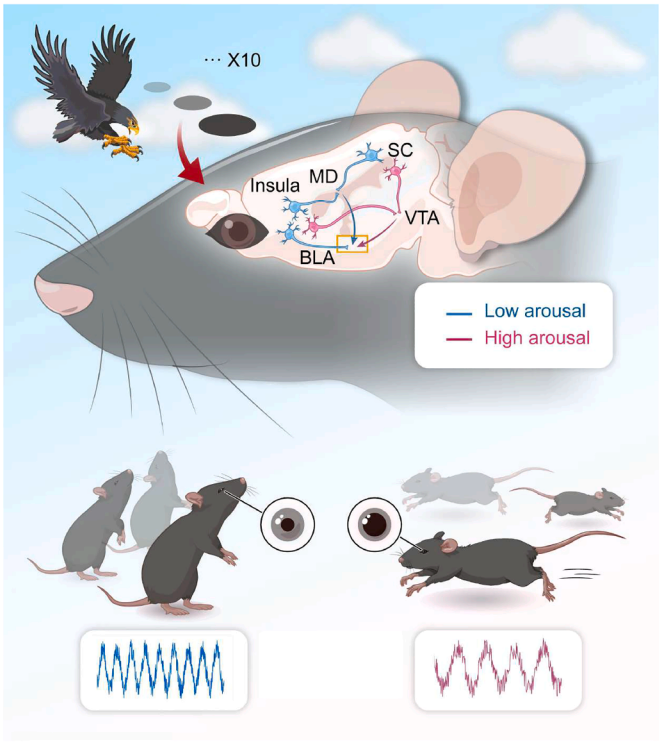


## Highlights

- Repeated looming revealed two distinct patterns of defensive behavior (T1 vs. T2)
- T1 involves SC/insula-VTA-BLA, while T2 relies on SC/insula-MD-BLA
- MD integrates SC and insula to regulate arousal and defense
- BLA beta oscillations contribute to regulating fear states

## Authors

Xuemei Liu, Juan Lai, Chuanliang Han, ..., Liming Tan, Fuqiang Xu, Liping Wang

## Correspondence

xm.liu@siat.ac.cn (X.L.), lp.wang@siat.ac.cn (L.W.)

## In brief

Liu et al. reveal distinct subcortical pathways from the superior colliculus to the amygdala and insula cortical pathways that govern two visual escape behaviors in two groups of mice, offering new insights into arousal modulation, internal states, and adaptive responses to visual threats.

Liu et al., 2025, Neuron *113*, 1–14
July 23, 2025 
https://doi.org/10.1016/j.neuron.2025.04.018

CellPress

Neuron

CellPress

Article

# Neural circuit underlying individual differences in visual escape habituation

Xuemei Liu,[1,2,3,4,5,6,*] Juan Lai,[1,2,6] Chuanliang Han,[1,2,6] Hao Zhong,[1,2] Kang Huang,[1,2] Yuanming Liu,[1,2] Xutao Zhu,[1,2] Pengfei Wei,[1,2,3,5] Liming Tan,[1,2,3,4] Fuqiang Xu,[1,2,3] and Liping Wang[1,2,3,4,5,7,*]

[1]CAS Key Laboratory of Brain Connectome and Manipulation, Shenzhen-Hong Kong Institute of Brain Science, Shenzhen Institute of Advanced Technology, Chinese Academy of Sciences, Shenzhen 518055, China

[2]Guangdong Provincial Key Laboratory of Brain Connectome and Behavior, Brain Cognition and Brain Disease Institute, Shenzhen Institute of Advanced Technology, Chinese Academy of Sciences, Shenzhen 518055, China

[3]University of Chinese Academy of Sciences, Beijing 10049, China

[4]Shenzhen Key Lab of Neuropsychiatric Modulation, Chinese Academy of Sciences, Shenzhen, Gudangdong 518055, China

[5]Key Laboratory of Brain Cognition and Brain-inspired Intelligence Technology, Center for Excellence in Brain Science and Intelligence Technology, Chinese Academy of Sciences, Shanghai, China

[6]These authors contributed equally

[7]Lead contact

*Correspondence: xm.liu@siat.ac.cn (X.L.), lp.wang@siat.ac.cn (L.W.)

https://doi.org/10.1016/j.neuron.2025.04.018

## SUMMARY

Emotions like fear help organisms respond to threats. Repeated predator exposure leads to adaptive responses with unclear neural mechanisms behind individual variability. We identify two escape behaviors in mice—persistent escape (T1) and rapid habituation (T2)—linked to unique arousal states under repetitive looming stimuli. Combining multichannel recording, circuit mapping, optogenetics, and behavioral analyses, we find parallel pathways from the superior colliculus (SC) to the basolateral amygdala (BLA) via the ventral tegmental area (VTA) for T1 and via the mediodorsal thalamus (MD) for T2. T1 involves heightened arousal, while T2 features rapid habituation. The MD integrates SC and insular cortex inputs to modulate arousal and defensive behaviors. This work reveals neural circuits underpinning adaptive threat responses and individual variability.

## INTRODUCTION

Emotional responses, such as fear behaviors, are evolutionarily conserved mechanisms hardwired into the brain to promote threat avoidance and ensure survival.[1–5] These responses are tightly regulated by internal states, which influence both the likelihood of specific defensive behaviors and the selection of appropriate strategies. Arousal, as a key component of internal states, plays a pivotal role in shaping adaptive responses to environmental challenges.[4,6–8] While singular predator encounters often trigger immediate defensive reactions, repeated exposures can elicit divergent coping strategies—habituation or sensitization—that are dependent on sensory inputs, internal states, and prior experiences.[9–12] The neural circuits underlying individual variability in internal state regulation and habituation to repeated threats remain poorly understood.

Visual looming stimuli (LS), which simulate an approaching predator, reliably evoke innate defensive responses across various species.[13–18] With repeated exposure, these stimuli often lead to habituation, an adaptive process that reduces the intensity of defensive responses and reflects the brain's ability to adjust to persistent threats.[19–23] Effective adaptive defense mechanisms necessitate a heightened state of awareness, an optimal level of arousal, and a focus on visually salient and biologically relevant stimuli. Previous research indicates that the magnitude and intensity of innate escape responses are influenced by external environmental factors and the organism's internal state.[24–31] Nonetheless, the circuit mechanisms underlying how arousal levels, internal states, and sensory salience interact to drive habituation to repeated LS remain poorly defined.

The superior colliculus (SC), a multimodal sensory processing hub, is essential for orienting, visual salience detection, and defensive responses.[32–36] The SC constitutes the subcortical route to the amygdala, a rapid "innate alarm system" bypassing cortical processing to promote threat avoidance.[36] SC-originating pathways include projections to the ventral tegmental area (VTA), essential for salience detection, motivation, and fear learning.[37–41] Additionally, the mediodorsal thalamus (MD), a downstream target of the SC, is involved in processing visual salience and arousal levels induced by sensory stimuli.[42–44] SC-VTA-amygdala pathway is well suited for facilitating fear learning and mediating habituation or dishabituation effects.[40] The SC-MD-amygdala pathway has been identified as mediating persistent fear attenuation, contributing to the underlying neurobiology that modulates visual-attentional processes.[45] However, the specific

Please cite this article in press as: Liu et al., Neural circuit underlying individual differences in visual escape habituation, Neuron (2025), https://doi.org/10.1016/j.neuron.2025.04.018



coordination of these distinct pathways in governing individual variability in defensive responses remains unclear.

The insula, a critical region for integrating interoceptive and emotional information, links internal states with external threats to guide decision-making and risk assessment.[46–50] Previous research demonstrates that the insula processes fear-related emotions by modulating the amygdala, a key node in subcortical pathways.[51–53] However, the coordination between the insular cortex and subcortical pathways that modulate defensive arousal and habituation to repeated predator exposures via the amygdala remains underexplored. Surprisingly, we found that approximately one-third of the mice (T2) exhibited rapid habituation characterized by low arousal (as indicated by decreased pupil size) but high attention levels (demonstrated by elevated rearing frequency [RF]) in response to repeated LS. Conversely, the remaining two-thirds of the mice (T1) consistently exhibited escape responses with corresponding arousal and rearing frequencies. Using a combination of optogenetics, *in vivo* multichannel recording, calcium imaging, and behavioral analyses, we demonstrate that the SC-VTA and insula-VTA pathways primarily mediate high-arousal escape behaviors, while the SC-MD and insula-MD pathways drive low-arousal habituation with enhanced sensory salience. These findings reveal how internal states, arousal, and attentional dynamics are orchestrated by discrete neural circuits to shape adaptive defensive behaviors. Our study not only clarifies the mechanisms underlying individual variability in habituation to threats but also offers novel insights into the interplay between neural circuits, behavioral adaptation, and internal state regulation.

## RESULTS

### Individual variability in escape habituation to repeated LS

Previous studies have established that LS reliably elicit innate escape behaviors. To explore the escape habituation to repeated LS, we exposed 52 wild-type (WT) adult male mice to 10 LS trials per session, with each trial lasting 5.5 s and interstimulus intervals (ISIs) of no less than 2 min (Figure 1A). Notably, our findings revealed individual differences in escape behavior. Only one mouse (~2%) exhibited no response, while the remaining 51 mice were categorized into two distinct response types. Mice initiating running in every trial with latency <5.5 s were designated as "consistent escape" (T1, $n$ = 35, 67.31%), and mice exhibiting ≥1 trial with a running latency ≥5.5 s were classified as T2 "rapid habituation" (T2, $n$ = 16, 30.77%) (Figure 1B). Compared with the T1 group, mice in the T2 group had a significantly lower average escape proportion (35.63% vs. 98.57%) (Figure 1C), exhibited longer average response latency (17.78 ± 1.10 s vs. 1.56 ± 1.10 s) and longer return time (19.86 ± 0.31 s vs. 2.91 ± 1.09 s), and spent less time in the nest (24.68 ± 0.59 s vs. 72.96 ± 1.15 s) (Figures 1F and 1G).

Analysis of average scores over trials revealed that the T2 group showed increased latency and time to return to the nest across initial, middle, and final trial phases (Figure S1).

Non-selective attention (NSA), characterized by scanning, orienting, and detecting stimuli, correlates with RF in novel settings.[54–56] The T2 group consistently exhibited higher RF across all trials compared with the T1 group (Figure 1D). Remarkably, in the T2 group, RF significantly increased following LS onset, in contrast to a decrease observed in the T1 group. No RF differences were noted between T1 and T2 groups before LS onset, indicating stimulus-specific RF patterns (Figure 1E). To assess arousal state, we performed pupillometry on head-fixed, awake mice placed on a ball treadmill (Figure 1H). Pupil size, measured 10 s post-LS onset, was significantly larger in the T1 group compared with the T2 group (Figures 1I–1K). No significant pupil size differences were observed between groups prior to or during LS exposure. Collectively, our results demonstrate that the T2 group, characterized by higher habituation, exhibits enhanced stimuli-evoked NSA and reduced arousal in response to repeated LS presentations.

### State-dependent activation of SC-MD and SC-VTA pathways drives distinct calcium dynamics

To elucidate the role of SC neurons activated during habituation to LS, we employed the Fos-targeted recombination in active populations 2 (FosTRAP2) technique.[57,58] On day 1, adeno-associated virus 5 (AAV5)-double-inverted orion (DIO)-EGFP was injected unilaterally into the SC of FosTRAP2 mice. On day 3, FosFRAP2 mice were injected with tamoxifen and exposed to repeated LS to activate TRAPed cells. On day 24, FosFRAP2 mice were exposed to LS again before perfusion (Figure 2A). Our results revealed a higher density of EGFP+ SC neurons in the T1 group compared with the T2 group, with looming-associated EGFP+ neurons showing increased activation in the intermediate layer (IL) and deep layer (DL), but not in the superficial layer (SL), suggesting the SC's role in promoting escape (Figures 2B and 2C). To further elucidate the functional roles of SC-VTA and SC-MD pathways in escape habituation, we aim to perform calcium imaging in T1 and T2 groups to compare activation patterns in the MD and VTA (Figures 2D–2F). Calcium imaging revealed significantly higher activation of the MD in the T2 group compared with the T1 group, indicating enhanced sensory processing. By contrast, the VTA showed greater activation in the T1 group than in the T2 group, highlighting its potential role in facilitating fear learning (Figures 2G and 2H). To investigate the activation of SC-MD and SC-VTA projections in T1 and T2 groups, we injected retro-Cre into the MD and VTA, followed by the injection of DIO-genetically encoded calcium indicator 7s (GCaMP7s) into the SC, with optical fibers implanted in the MD and VTA (Figures 2I and 2J). Our results showed that LS elicited stronger activation of SC-MD projections in the T2 group compared with T1, whereas SC-VTA projections exhibited greater activation in the T1 group compared with T2 (Figures 2K and 2L). These findings suggest that the T1 group predominantly engages the SC-VTA pathway to facilitate fear learning, while the T2 group relies more on the SC-MD pathway to process sensory salience and arousal.

### VTA-projecting and MD-projecting SC neurons functionally target the BLA

The amygdala, particularly the basolateral amygdala (BLA), is crucial for integrating and encoding threat-related information. The BLA plays a central role in fear learning by associating sensory stimuli with aversive outcomes and regulating fear memory.

Please cite this article in press as: Liu et al., Neural circuit underlying individual differences in visual escape habituation, Neuron (2025), https://doi.org/10.1016/j.neuron.2025.04.018



CellPress

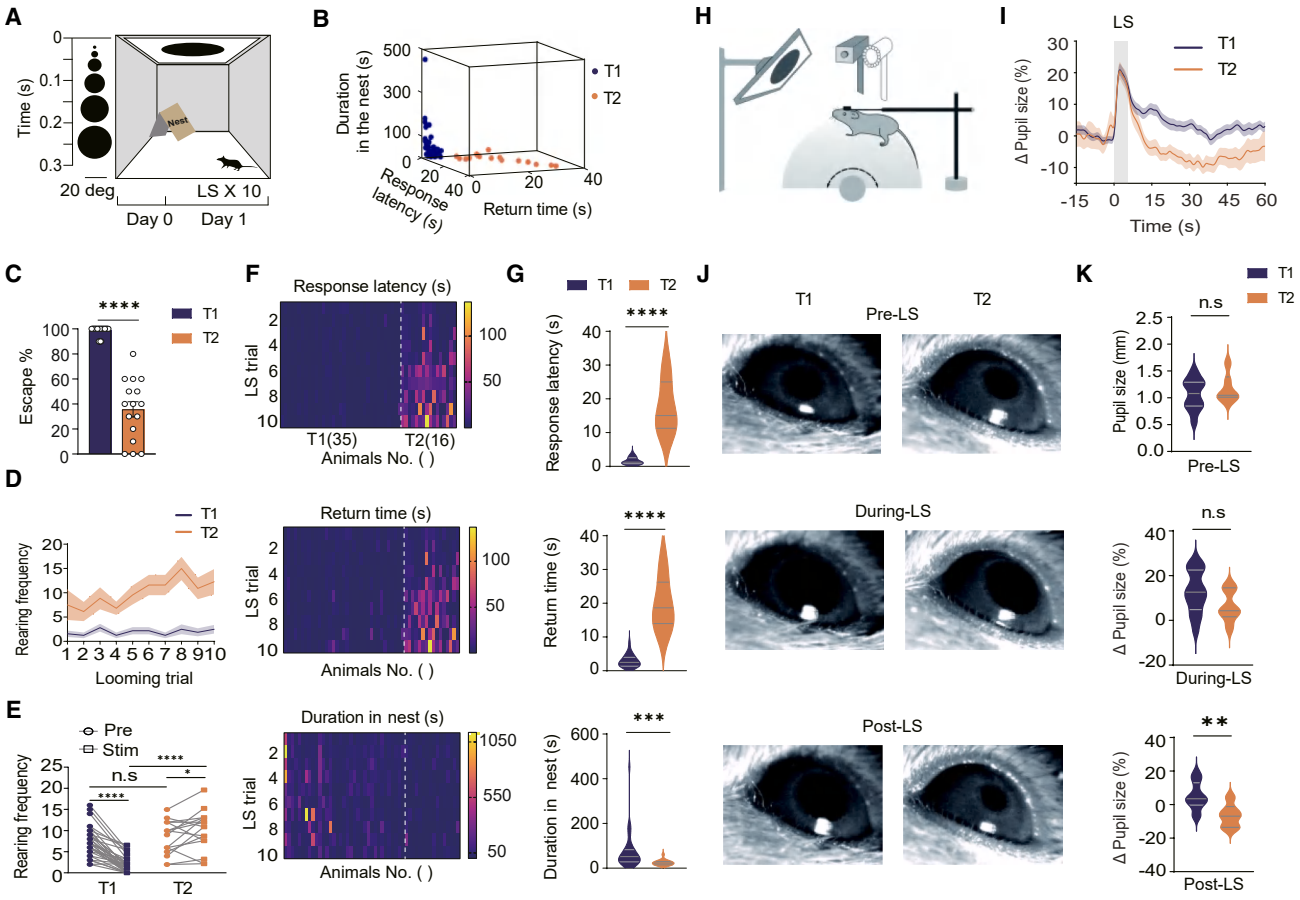


**Figure 1. Individual variability in escape habituation to repeated looming stimuli**

(A) Schematic of LS paradigm and timeline with expanding dark disk and randomized ISIs

(B) Three-dimensional (3D) scatterplot of escape parameters (latency, return time, nest duration) for T1 ("consistent escape") and T2 ("fast habituation") mice. T1, $n = 35$ mice; T2, $n = 16$ mice.

(C) Average escape trial proportion for T1 and T2 mice.

(D) RF comparison across trials for T1 and T2 mice.

(E) RF pre-LS vs. during LS for T1 and T2 mice.

(F) Heatmap of escape parameters across trials for 51 mice.

(G) Bar graph of average escape parameters (latency, return time, nest duration) for T1 and T2 mice during LS.

(H) Schematic of pupillometry paradigm during LS in head-fixed mice.

(I) Percent pupil-size change pre- and post-LS for T1 and T2 mice.

(J and K) Pupil size pre-LS, during LS, and post-LS.

Additionally, it processes sensory salience and arousal, shaping behavioral and physiological responses to threats.[3,59] We investigated whether SC neurons projecting to the VTA and the MD converge on the BLA. Using AAV1-mediated anterograde transsynaptic tagging,[60] we injected AAV1-Cre into the SC, followed by injections of AAV5-DIO-EYFP into the MD and AAV5-DIO-mCherry into the VTA (Figure 3A). Cre expression revealed overlapping axonal projections in the BLA, indicating that both VTA-projecting and MD-projecting SC neurons innervate a common region within the BLA (Figure 3B). Fluorescence density analysis showed that VTA-projecting SC neurons primarily innervated the medial BLA, while MD-projecting neurons targeted the anterior and posterior parts (Figure 3C). These findings suggest that the BLA acts as a downstream integrative hub for SC-MD and SC-VTA pathways, processing their distinct sensory and arousal-related signals.

## SC pathways modulate BLA oscillations and pupil-linked arousal

To further examine how these pathways regulate threat encoding and neural dynamics in the BLA, we combined *in vivo* multichannel and eye movement recordings following selective activation or inhibition of SC-MD and SC-VTA projections (Figure 4A). This approach revealed their distinct contributions to arousal-related oscillatory activity and fear learning in the BLA.

To dissect the functional roles of these pathways, we used AAV5-calcium/calmodulin-dependent kinase II alpha (CaMKIIα)-channelrhodopsin 2 (ChR2)-mCherry injections into

Please cite this article in press as: Liu et al., Neural circuit underlying individual differences in visual escape habituation, Neuron (2025), https://doi.org/10.1016/j.neuron.2025.04.018



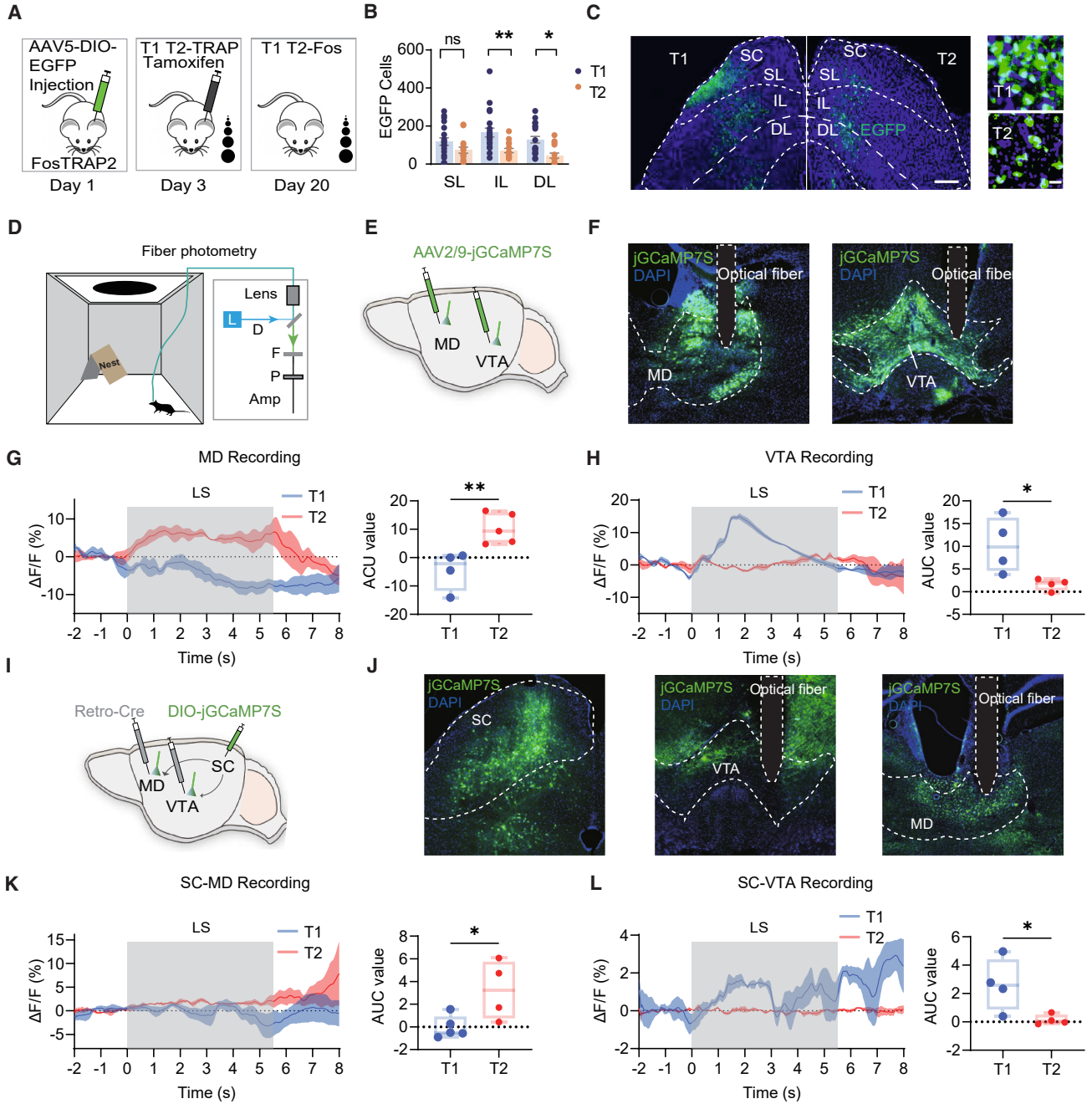


**Figure 2. State-dependent activation of SC-MD and SC-VTA pathways drives distinct calcium dynamics**

(A) Schematic illustrating the FosTRAP2 procedure.

(B and C) Looming-associated EGFP+ neurons in SC layers (SL, superficial layer; IL, intermediate layer; DL, deep layer) in T1 and T2 mice.

(D–F) Schematics of *in vivo* fiber photometry and AAV-GCaMP7S virus expression in the MD and VTA.

(G and H) Calcium responses and statistical comparisons of MD and VTA neurons during LS in T1 and T2 mice.

(I and J) AAV-retro-Cre virus injection into MD and VTA, and AAV-DIO-GCaMP7S virus expression in SC.

(K and L) Calcium responses and statistical comparisons of SC-MD and SC-VTA neurons during LS in T1 and T2 mice.

the SC with optic fiber implantation in the MD and VTA for activation (Figure S3E) and selectively inhibited SC-MD and SC-VTA circuits by injecting retro-Cre into the MD or VTA and DIO-Guillardia theta anion channelrhodopsin 2 (GtACR2) into the SC (Figure 4F). We performed pupillometry on head-fixed mice. Optogenetic activation (473 nm, 2.5 s, 20 Hz, 50 pulses) altered pupil size, revealing distinct effects on pupil response. Activation of the SC-MD pathway induced pupil constriction,

Please cite this article in press as: Liu et al., Neural circuit underlying individual differences in visual escape habituation, Neuron (2025), https://doi.org/10.1016/j.neuron.2025.04.018



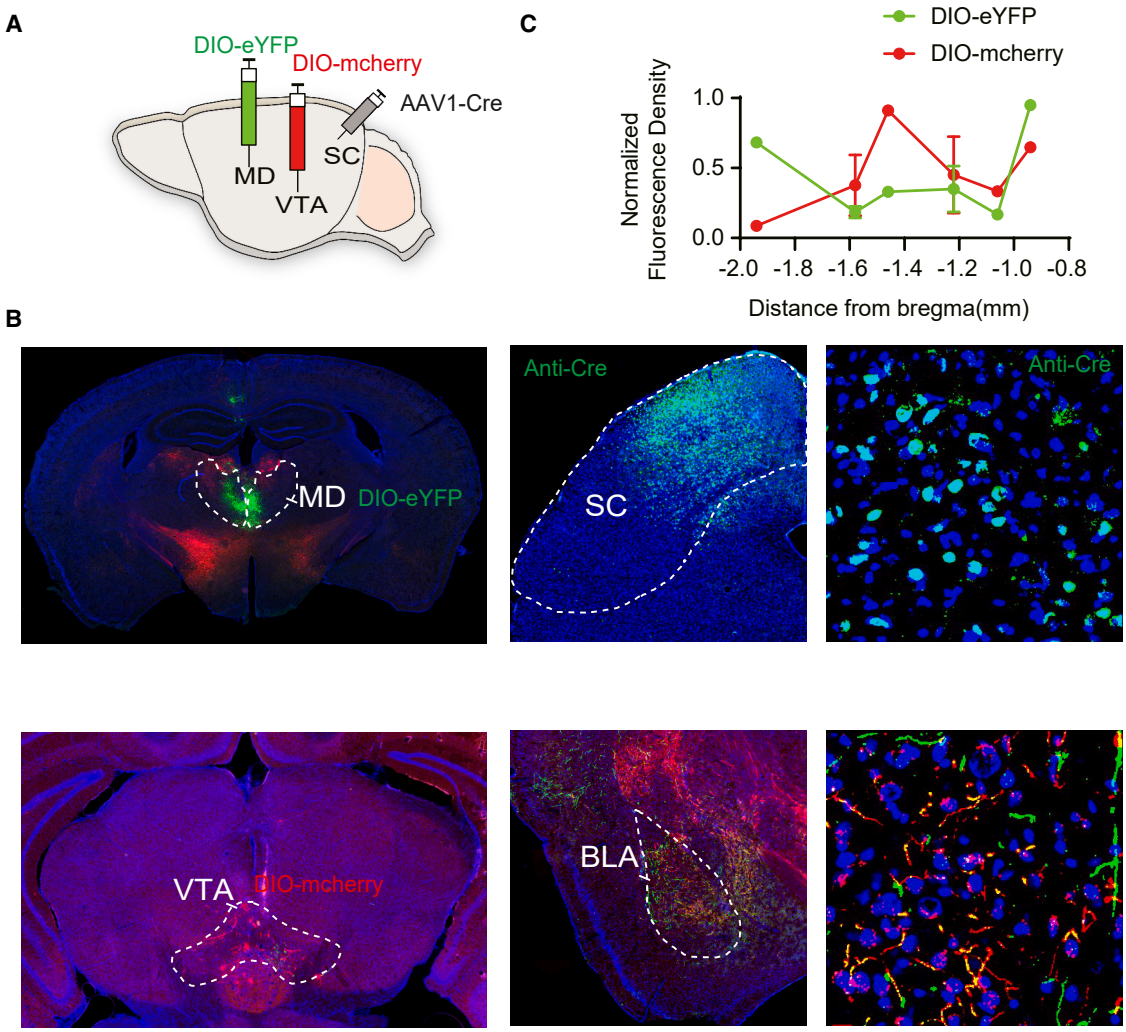


**Figure 3. VTA-projecting and MD-projecting SC neurons target the BLA**

(A) Schematic showing injections of AAV1-Cre into the SC and AAV5-DIO-mCherry and AAV5-DIO-EYFP into the VTA and the MD.

(B) Representative images showing AAV1-Cre virus injection and Cre immunopositive expression in the SC, AAV5-DIO-EYFP in the MD, AAV5-DIO-mCherry in the VTA, and fiber terminals in the BLA. Scale bars, 250 (left), 100 (middle), and 10 (right) μm.

(C) Normalized fluorescence density of fibers labeled with mCherry and EYFP in the BLA.

whereas SC-VTA stimulation led to pupil dilation (Figures 4B–4E). Conversely, inhibiting these pathways produced opposite effects: SC-VTA inhibition led to pupil constriction, and SC-MD inhibition resulted in pupil dilation (Figures 4G–4J). Notably, baseline pupil size before optogenetic stimulation (OS) did not differ significantly between groups, but during and after OS, the SC-VTA group exhibited significantly larger pupil sizes compared with the SC-MD group (Figures 4B–4E). Using simultaneous pupillometry and *in vivo* multichannel recording in the BLA, we observed pathway-specific effects on oscillatory activity. SC-VTA activation enhanced theta and alpha power in the BLA, while SC-MD activation primarily increased beta and low gamma power (Figures 4K–4M). Neuronal firing rates within the BLA significantly changed following pathway activation or inhibition: SC-MD activation affected 11% of neurons (9% excitation, 2% inhibition), while SC-VTA activation affected 9% (7% excitation, 2% inhibition). By contrast, SC-MD inhibition led to 14% excitation and 3% inhibition, whereas SC-VTA inhibition resulted in 27% excitation and less than 1% inhibition. These results demonstrate distinct and pathway-specific influences on BLA neuronal activity (Figures S4–S7). Interestingly, inhibiting the SC-VTA pathway resulted in heightened beta, low gamma, and high gamma power, suggesting a compensatory shift in arousal-related neural dynamics (Figures 4N–4P). These findings highlight the distinct roles of SC-VTA and SC-MD pathways in regulating arousal, sensory processing, arousal-linked neural oscillations, and threat learning mechanisms in the BLA.

## SC pathways differentially shape looming escape responses

Considering the larger pupil size in the T1 group and following SC-VTA activation, we hypothesized that repeated SC-VTA

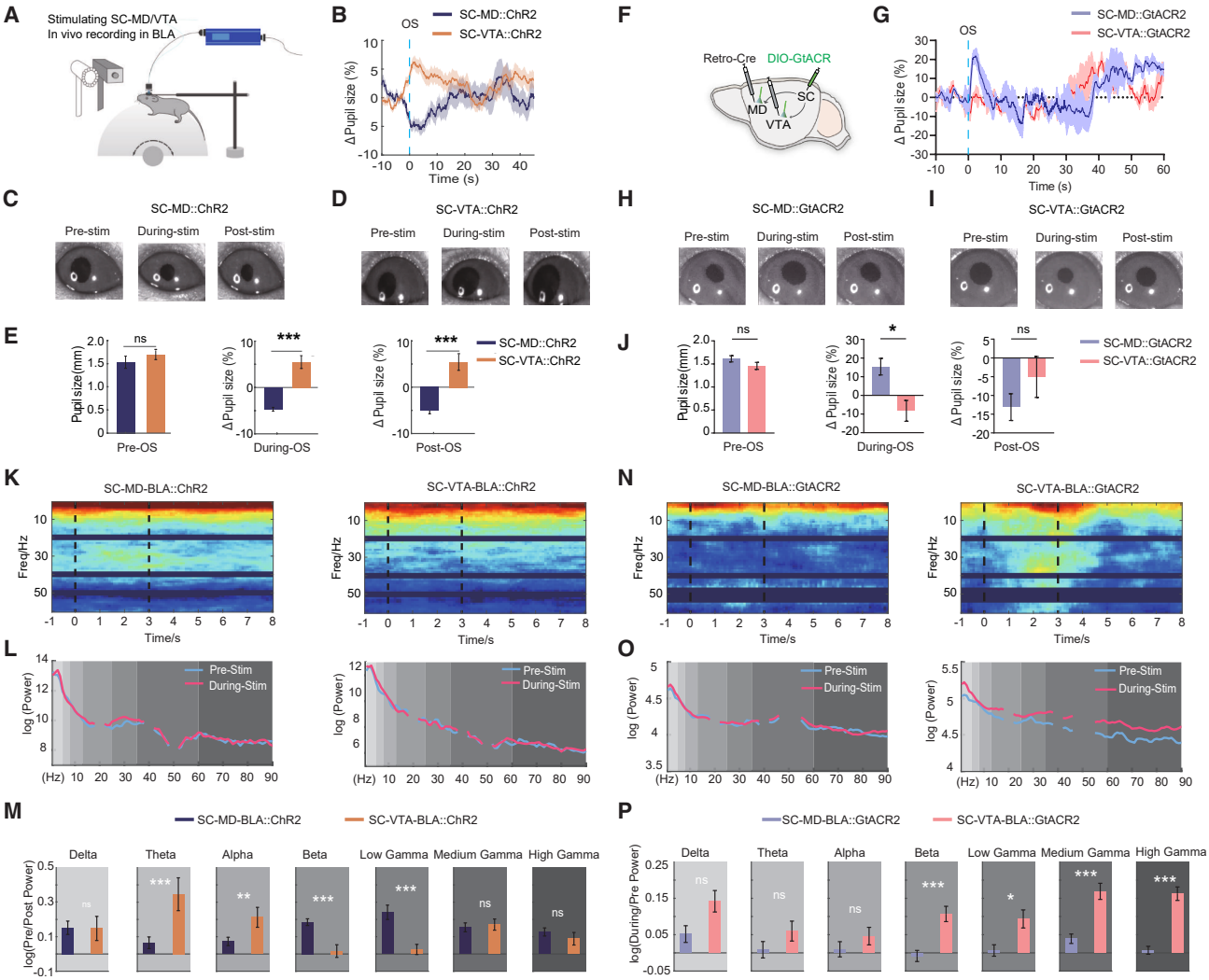


**Figure 4. SC-MD and SC-VTA circuit activation or inhibition modulates change in pupil size and BLA oscillatory dynamics**

(A) Schematic of electrophysiological recordings of SC-VTA and SC-MD targeting the BLA, with pupil size monitored via eye tracking.

(B–E) Graphs of normalized pupil size before, during, and after OS under optogenetic activation of SC-MD and SC-VTA pathways.

(F) AAV-retro-Cre injection into MD and VTA, with AAV-DIO-GtACR2 expression in SC.

(G–J) Pupil size analysis (B–E) repeated under optogenetic inhibition of the SC pathway.

(K and L) Local field potential (LFP) and power spectrograms in the BLA during optogenetic activation of SC-MD and SC-VTA.

(M) LFP power comparison across frequency bands before, during, and after SC-MD and SC-VTA activation.

(N–P) LFP and power analyses (K–M) repeated under optogenetic inhibition of the SC pathway.

stimulation would elicit T1-like behavior. Indeed, repeated SC-VTA OS resulted in stable escape behavior in an open field with shelter, mimicking T1 group responses (Figure S2).

To map SC projections, we injected rabies virus (RV) conjugated with dsRed into the VTA and RV-EGFP into the MD, allowing us to quantify labeled neurons across the brain. Among the retrogradely labeled neurons in the SC, 51% projected to the MD, 63% projected to the VTA, and 14.4% were co-labeled, indicating that some SC neurons send collaterals to both the MD and VTA (Figure S3).

To assess whether collateral projections influence behavior, we blocked SC action potential backpropagation with 0.3 μL of 4% bupivacaine.[61] This manipulation did not alter behavioral responses during activation of either the SC-VTA or SC-MD pathway in the open field with shelter paradigm (Figure S3). These results suggest that SC pathways operate in parallel to modulate variability in innate escape responses, rather than through shared collateral effects.

Further investigations assessed the SC pathways' roles via ChR2-mCherry expression in SC neurons during looming stimulation. SC-MD OS increased RF, response latency, and return time, but SC-VTA OS did not, indicating that SC-MD OS disrupts looming-induced escape behaviors. Thus, SC-MD activation

Please cite this article in press as: Liu et al., Neural circuit underlying individual differences in visual escape habituation, Neuron (2025), https://doi.org/10.1016/j.neuron.2025.04.018



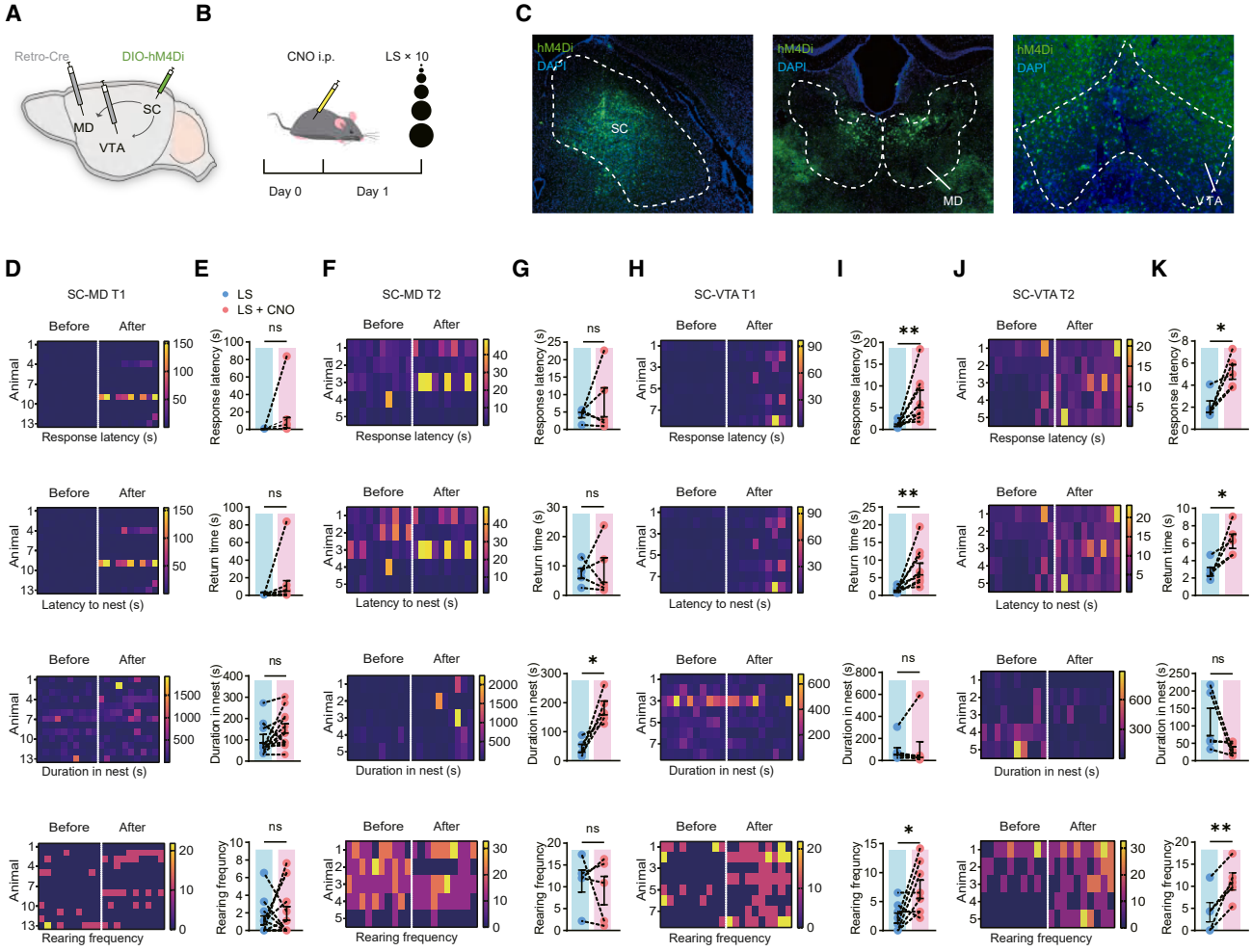


**Figure 5. Effects of SC-MD and SC-VTA circuit inhibition on response patterns to repeated LS in T1 and T2 mice**

(A–C) Schematic of AAV-retro-Cre injection into MD and VTA, with AAV-DIO-HM4Di expression in SC.

(D and E) Heatmap and bar graph of escape behavior parameters during SC-MD circuit inhibition in T1 mice.

(F and G) Same as (D) and (E) for T2 mice.

(H and I) Heatmap and bar graph of escape behavior parameters during SC-VTA circuit inhibition in T1 mice.

(J and K) Same as (H) and (I) for T2 mice.

Scale bar differences were applied to better display the data points.

decreased arousal and increased NSA, impairing innate escape, whereas SC-VTA activation increased arousal without affecting NSA or escape behavior (Figures S3E–S3G). These findings suggest that precise optogenetic control of arousal states can ultimately modulate decision-making during fear responses.

To explore the roles of SC-MD and SC-VTA pathways in regulating behavioral responses to repeated LS across T1 and T2, we employed chemogenetic inhibition. AAV-retro-Cre was injected bilaterally into the MD and VTA, and DIO-human muscarinic receptor 4 designer receptor inhibitory (hM4Di) into the SC. Behavioral changes were compared before and after clozapine-N-oxide (CNO) administration (Figures 5A–5C).

Inhibition of the SC-VTA pathway broadly impacted both T1 and T2 groups, altering escape and learning-related behaviors (Figures 5H–5K). By contrast, SC-MD inhibition specifically increased nesting duration in T2 animals, with no effect on T1 behaviors or T2 parameters like response latency or return time and RF (Figures 5D–5G). These findings reveal distinct functional contributions of SC-VTA and SC-MD pathways in shaping defensive behaviors. The SC-VTA pathway exhibits a generalized influence across different phenotypes, while the SC-MD pathway exerts a more targeted effect on context-dependent duration in nest in T2 animals. Together, these results highlight the nuanced interplay between SC subcircuits in orchestrating adaptive responses to environmental threats.

## Distinct insular cortex circuits orchestrate BLA oscillations and pupil-linked arousal

The insular cortex integrates sensory feedback and autonomic arousal, linking internal states to environmental cues.[46–50] Its

Please cite this article in press as: Liu et al., Neural circuit underlying individual differences in visual escape habituation, Neuron (2025), https://doi.org/10.1016/j.neuron.2025.04.018



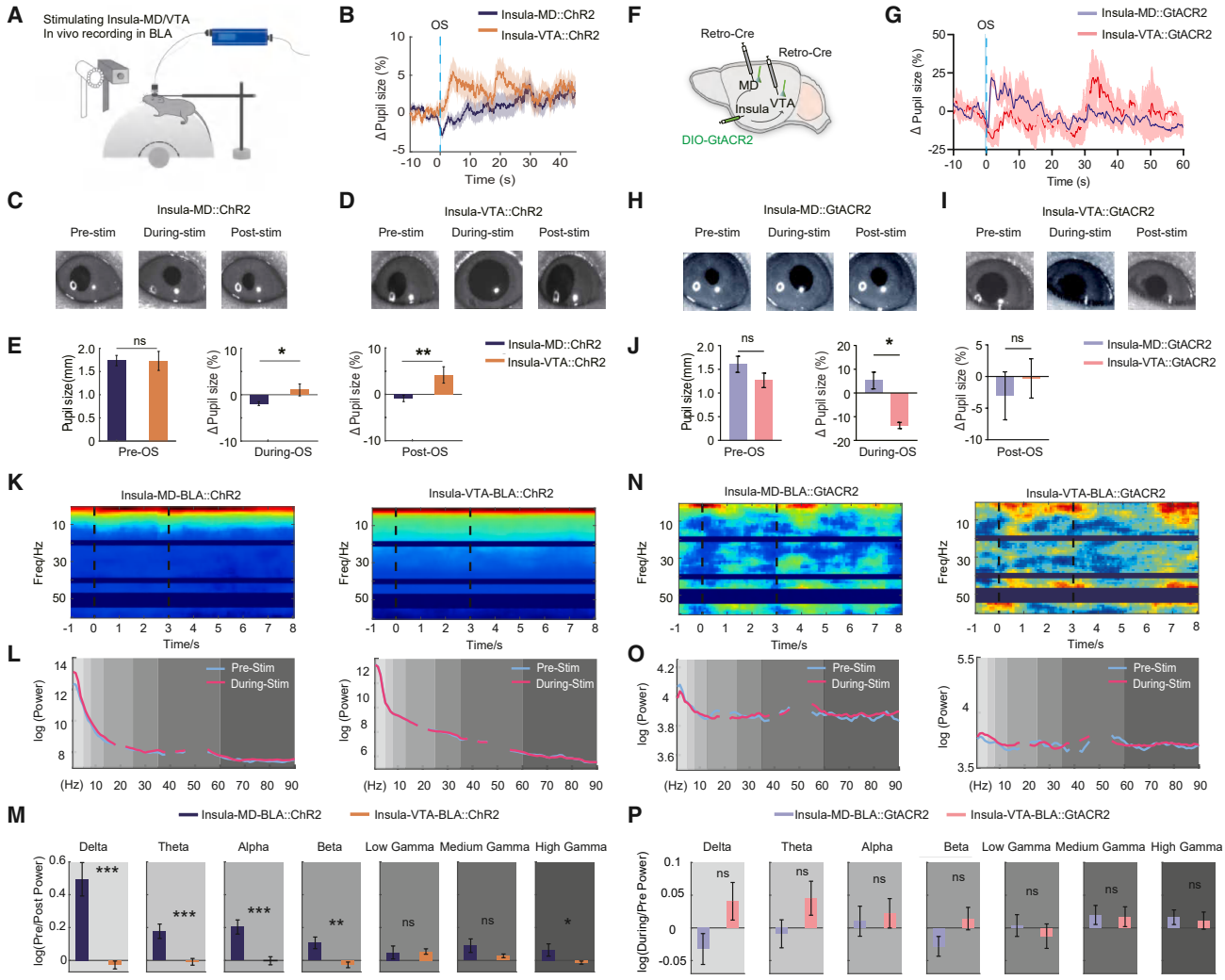


**Figure 6. Insula-MD and insula-VTA circuit activation or inhibition modulates pupil size and BLA oscillatory dynamics**

(A) Schematic of electrophysiological recordings targeting insula-VTA and insula-MD projections to the BLA, with pupil size monitored via eye tracking.

(B–E) Graphs of normalized pupil size before, during, and after OS under optogenetic activation of insula-MD and insula-VTA pathways.

(F) AAV-retro-Cre injection into MD and VTA, with AAV-DIO-GtACR2 expression in the insular cortex.

(G–J) Pupil size analysis (B–E) repeated under optogenetic inhibition of the insular pathway.

(K and L) LFP and power spectrograms in the BLA during optogenetic activation of insula-MD and insula-VTA pathways.

(M) Bar graph comparing LFP power across frequency bands before, during, and after activation of insula-MD and insula-VTA pathways.

(N–P) LFP and power analyses (K–M) repeated under optogenetic inhibition of the insular pathway.

projections to the MD and VTA enable dual regulation of arousal states and behaviors (Figure S3). Investigating insula circuits reveals how cortical mechanisms influence instinctive defensive decisions. This approach bridges cortical processing with subcortical arousal centers, offering insights into fear and stress regulation.

To further elucidate the functional roles of insula-VTA and insula-MD pathways in escape habituation, retro-Cre was injected into the MD and VTA, followed by DIO-GCaMP7s injection into the insula, with optical fibers implanted in the MD and VTA (Figures S8A–S8C). LS evoked stronger activation of insula-MD projections in T2, while insula-VTA projections exhibited greater activation in T1 (Figures S8D and S8E). T1 predominantly relies on the insula-VTA pathway, reflecting the insula's role in integrating emotional and interoceptive signals to drive defensive behaviors. By contrast, T2 engages the insula-MD pathway, highlighting its function in attention regulation and cognitive processing.

To dissect the functional roles of these pathways, AAV5-CaMKIIα-ChR2-mCherry was injected into the insula, with optical fibers implanted in the MD and VTA for activation (Figure S13). Retro-Cre was injected into the MD or VTA along with DIO-GtACR2 into the insula for circuit-specific inhibition (Figure 6F). Pupillometry in head-fixed mice revealed pathway-specific effects on pupil responses: insula-MD activation

Please cite this article in press as: Liu et al., Neural circuit underlying individual differences in visual escape habituation, Neuron (2025), https://doi.org/10.1016/j.neuron.2025.04.018



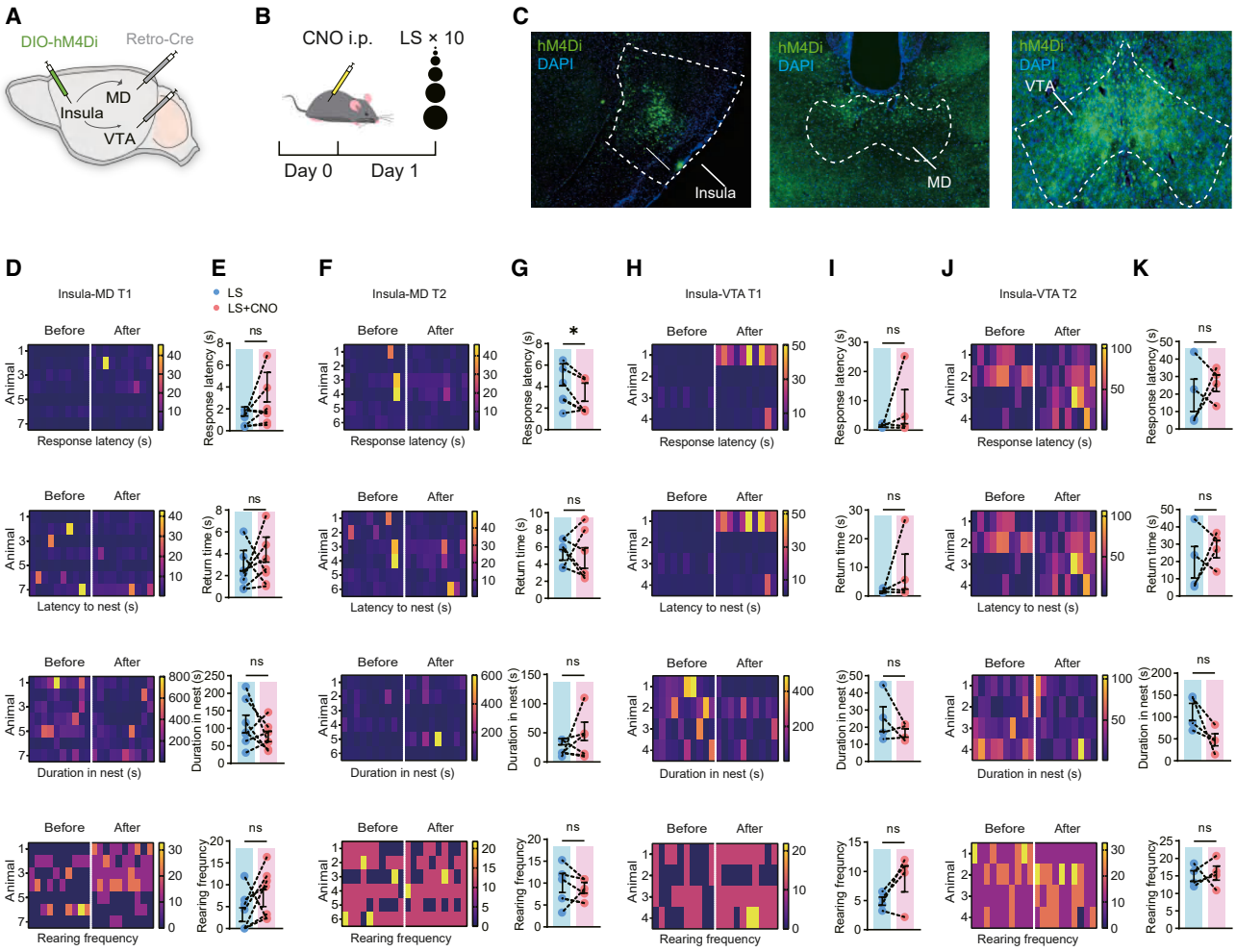


**Figure 7. Effects of SC-MD and SC-VTA circuit inhibition on response patterns to repeated LS in T1 and T2 mice**

(A–C) Schematic of AAV-Retro-Cre injection into MD and VTA, with AAV-DIO-HM4Di expression in insular cortex.

(D and E) Heatmap and bar graph of escape behavior parameters during insula-MD circuit inhibition in T1 mice.

(F and G) Same as (D) and (E) for T2 mice.

(H and I) Heatmap and bar graph of escape behavior parameters during insula-VTA circuit inhibition in T1 mice.

(J and K) Same as (H) and (I) for T2 mice.

induced pupil constriction, while insula-VTA activation caused pupil dilation. Conversely, inhibiting these pathways produced opposite effects (Figures 6G–6J).

Baseline pupil size was comparable between groups, but during and after OS, the insula-VTA group exhibited larger pupil sizes compared with the insula-MD group (Figures 6B–6E). Simultaneous pupillometry and BLA multichannel recordings showed pathway-specific effects on oscillatory activity: insula-MD activation increased delta, theta, alpha, and beta power (Figures 6K and 6L). However, inhibiting the insula-VTA pathway and the insula-MD pathway resulted in no significant differences in BLA local field potential (LFP) changes (Figures 6N–6P). Neuronal firing rates within the BLA showed pathway-specific changes following insula activation or inhibition: insula-MD activation affected 30% of neurons (8% excitation, 22% inhibition), while insula-VTA activation affected 20% excitation and <1% inhibition. Inhibition of insula-MD led to 10% excitation and 3% inhibition, whereas insula-VTA inhibition caused 16% excitation and 3% inhibition, highlighting distinct regulatory roles (Figures S9–S12).

To investigate pathway involvement during LS presentations, AAV5-CaMKIIα-ChR2-mCherry was injected into the insular cortex, with optical fibers targeting the MD and VTA (Figures S13A and S13B). Insula-MD activation increased RF, response latency, and return time while reducing nest time, indicating decreased arousal, which dampened LS-induced escape. By contrast, insula-VTA activation heightened arousal but did not alter escape behaviors (Figures S13C and S13D).

These findings highlight the insula's role in regulating arousal and attention, with insula-MD suppressing escape via reduced arousal and insula-VTA heightening arousal without affecting escape, contrasting the SC's direct sensory-motor function.

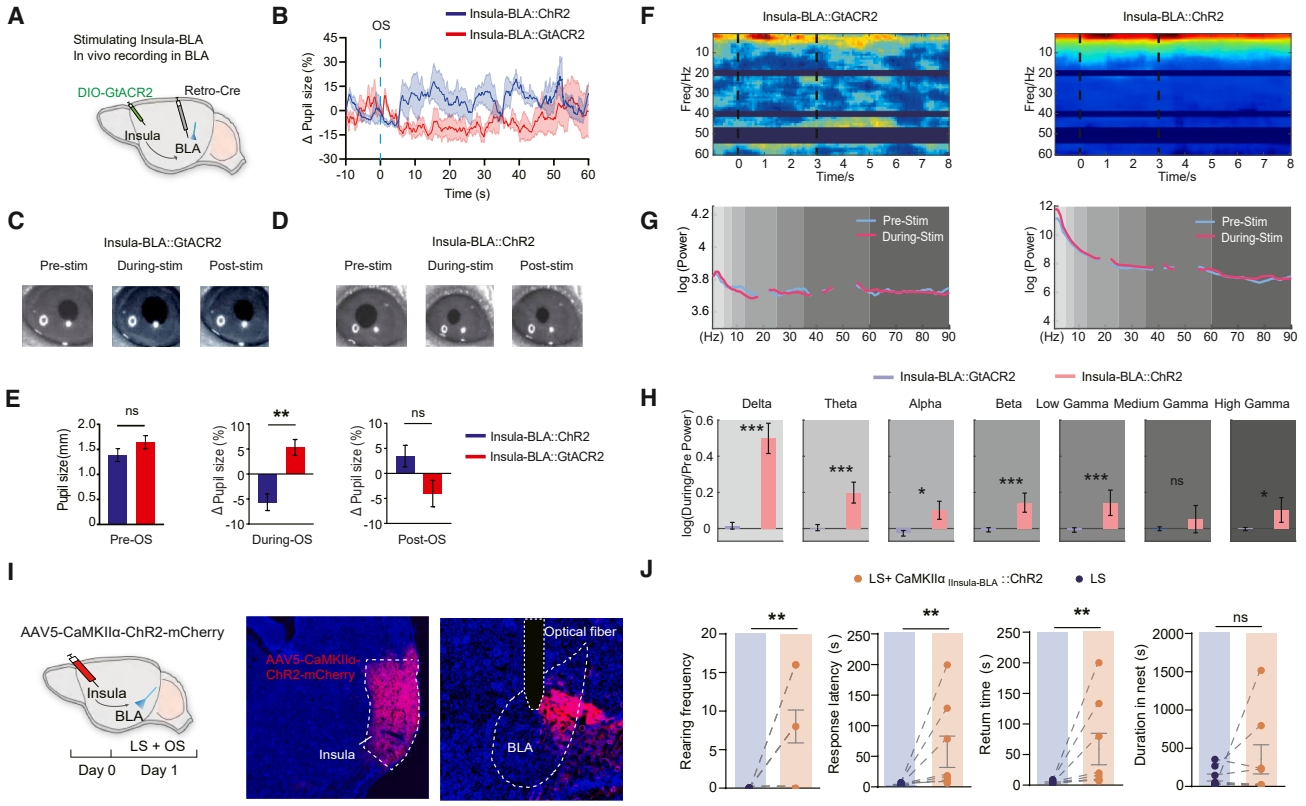


**Figure 8. Insula-BLA activation abolishes fear via enhancing pupil constriction and amygdala activity**

(A and B) Schematic showing electrophysiological recording of insula-BLA pathway modulation and an eye tracker to monitor the pupil size.

(C–E) Graph showing normalized pupil size before OS, during OS, and after OS under optogenetic activation insula-BLA pathway. OS, opto-stimulation.

(F and G) LFP and power spectrograms recorded in the BLA during optogenetic activation and inhibition insula-BLA pathway.

(H) Bar graph comparing LFP power across different frequency bands before, during, and after optogenetic activation and inhibition insula-BLA pathway.

(I and J) Measurements were taken during OS (10 trials/mouse) and LS of CaMKIIα$_{insula\text{-}BLA}$::ChR2 mice. Bar graphs showing (1) rearing frequency, (2) response latency, (3) return time, and (4) duration in nest.

To investigate the specific contributions of the insula-MD and insula-VTA pathways to escape habituation, we examined the effects of their inhibition in both T1 and T2 animals (Figures 7A–7C). Inhibition of the insula-MD pathway had no effect on T1 behaviors but specifically reduced response latency in T2 animals, indicating its role in facilitating more rapid responses to threats under repeated exposure (Figures 7D–7G).

By contrast, inhibition of the insula-VTA pathway had no measurable effect on either T1 or T2 animals (Figures 7H–7K). These results highlight that the insula-MD pathway enhances response efficiency under repeated threats, likely reflecting its role in adaptive timing and decision-making. By contrast, the insula-VTA pathway does not significantly contribute to the observed defensive behaviors, emphasizing pathway-specific functions in threat responses.

## Insular cortex directly governs BLA oscillations and arousal-linked responses

To explore whether the insula directly regulates pupil dynamics, modulates BLA activity, and influences defensive decision-making, we employed a combination of *in vivo* recordings, pupillometry, and targeted manipulations of the insula-BLA pathway (Figure 8A). Activation of this pathway induced significant pupil constriction, whereas inhibition resulted in pupil dilation (Figures 8B–8D). Furthermore, compared with pathway inhibition, excitation of the insula-BLA pathway robustly increased BLA oscillatory power across delta, theta, alpha, beta, and low-gamma frequency bands, demonstrating enhanced modulation of BLA network dynamics (Figures 8F–8H). Insula-BLA activation affected 52% of neurons (40% excitation, 2% inhibition), while the inhibition of this pathway affected 9% excitation and 3% inhibition (Figures S14 and S15). To assess the pathway's role in defensive behaviors, we stimulated the insula-BLA pathway during looming stimulus presentations. Using retro-Cre injections into the BLA paired with DIO-hM4Di injections into the insula, pathway-specific inhibition was achieved via CNO administration. Excitation of the insula-BLA pathway significantly altered defensive responses, whereas inhibition had no measurable impact on escape behaviors in T1 or T2 mice (Figure S16). These findings reveal that the insula-BLA pathway directly modulates both pupil dynamics and BLA activity, exerting a selective influence on defensive decision-making.

Please cite this article in press as: Liu et al., Neural circuit underlying individual differences in visual escape habituation, Neuron (2025), https://doi.org/10.1016/j.neuron.2025.04.018



## DISCUSSION

In the study, we found that rodents exhibit two types of behavioral responses to repeated LS: consistent escape (T1) and rapid habituation (T2), each characterized by distinct pupil sizes and rearing frequencies. Additionally, we identified divergent pathways originating from the SC and the insula, which project to BLA and contribute to different levels of defensive arousal and habituation responses to repeated LS. Furthermore, the state of defensive arousal and the manipulation of separate circuits play distinct roles in regulating the power of LFP in the BLA. This research enhances our understanding of how internal states, such as arousal and fear, are modulated at the neural level and highlights the complexity of these processes.

### Distinct neural pathways governing behavioral responses

Individual differences are crucial as they supply the raw materials for natural selection, as evidenced by the variability in individual adaptations to repeated predator encounters.[62,63] The behavioral adaptation needs optimizing perception and attention by conserving cognitive resources and enhancing biological salience detection, thereby enabling threat detection and resilience.[52,64] The SC's well-documented functions in detecting and directing attention to salient visual stimuli align with its involvement in both T1 and T2 behaviors. In T1, consistent escape behavior is driven by sustained activation of the SC-VTA-amygdala pathway, maintaining the high arousal needed for continuous defensive responses, which, despite its energy cost, this sensitization-like response enhances survival probability in environments with unpredictable threats.[65] This pathway's role in reinforcement fear learning and mediating potential sensitization or dishabituation effects is consistent with its established contributions to innate defensive responses and motivational control.[32,37]

Conversely, T2 behavior involves rapid habituation via transient SC-MD-amygdala pathway or insula-MD-amygdala pathway activation, swiftly reducing arousal and defensive responses.

This rapid habituation aligns with previous studies in larval zebrafish, crabs, and other species,[21,23,66] enabling animals to disregard irrelevant stimuli and focus on biologically significant threats, thereby enhancing adaptive survival by reducing responses to non-threatening cues. The SC also influences higher-order regions by directing attention in a bottom-up manner.[67–69] These findings underscore the role of a "visual salience network," comprising subcortical pathways and top-down cortical visuomotor control, in coordinating visual attention toward novel, salient stimuli and unexpected threats.[49,70] T2 behaviors rely on rapid habituation mediated by the SC-MD-BLA and insula-MD-BLA pathways, which transiently reduce arousal and defensive responses. These mechanisms filter out irrelevant stimuli, enable cognitive resource conservation, and enhance attention to biologically significant threats, providing an evolutionary advantage in environments with predictable threats.

### The role of the MD as a central hub

The MD emerged as a central node integrating inputs from both the SC and insula to regulate amygdala activity. MD circuitry modulates both beta oscillations and behavioral outputs, facilitating the attenuation of fear responses via its projections to the amygdala. This centrality underscores the importance of the MD in balancing arousal and attentional states to maintain behavioral flexibility in dynamic environments. Such flexibility allows animals to optimize energy expenditure while maintaining vigilance, a critical evolutionary trade-off for survival.

### Arousal, fear attenuation, pathway-specific oscillatory dynamics

Our findings investigate how the SC and insula pathways modulate BLA oscillations and pupil-linked arousal, and amygdala beta oscillations (12–30 Hz) emerged as a key marker of escape habituation and pupil constriction. Activation of the SC-MD, insula-MD, and insula-BLA pathways consistently enhanced beta power, correlating with pupil constriction and reduced defensive responses, whereas inhibition of these pathways reversed these effects. By contrast, other oscillatory patterns lacked consistency. For instance, insula-MD activation increased delta (1–4 Hz), theta (4–7 Hz), and alpha (8–12 Hz) power, while SC-MD activation reduced them. Despite these differences, both pathways resulted in similar behavioral outcomes—pupil constriction and fear reduction—suggesting that delta, theta, and alpha oscillations may not be directly associated with fear attenuation. These findings suggest that beta oscillations contribute to the modulation of fear responses within a broader network context[71] while highlighting the functional specialization of distinct frequency bands. Beta oscillations may reflect synchronized inhibitory inputs, stabilizing neural activity and preventing excessive excitation during fear habituation. This contrasts with the role of gamma, delta, theta, and alpha oscillations, whose effects appear pathway specific and may encode other emotional or attentional dimensions of threat adaptation.

### Translational potential

Maladaptive behaviors in response to extreme fear can lead to either heightened sensitivity to harmless stimuli (overreaction) or reduced detection and response to actual threats (underreaction).[1,72,73] In humans, these responses are common in fear-related disorders such as phobias, anxiety, post-traumatic stress disorder (PTSD), and delusional disorders. The selective involvement of beta oscillations in fear attenuation provides a targetable mechanism for regulating these pathological responses. Therapeutic interventions aimed at modulating beta oscillatory activity, potentially through neuromodulation or pharmacological approaches, may offer new avenues for treating fear-related disorders.

Our findings have significant implications for understanding individual variability in emotional processing and resilience. The ability to rapidly habituate to repeated threats could confer advantages in certain environments, reducing stress-related pathologies. Conversely, a consistent escape response might be advantageous in environments where threats are unpredictable and potentially lethal. Understanding the neural circuits and molecular mechanisms behind individual differences in habituation to repeated predator exposures could inform personalized treatments for neuropsychiatric conditions.[36] By concentrating on

evolutionarily conserved circuits like the SC-MD-amygdala pathway, our research establishes a physiological basis for developing potential therapies. Further detailed analysis of the molecular mechanisms of the subcortical pathway could enhance the translational value of research by identifying a key target for PTSD treatment.[45,74,75]

## Limitations of the study

This study highlights the role of SC- and insula-mediated circuits in fear habituation but has limitations. The molecular mechanisms linking beta oscillations to excitation-inhibition dynamics and the roles of delta, theta, and alpha oscillations remain unclear, necessitating further causal investigations. While pupil size is a robust arousal correlate, incorporating measures like heart rate variability or hormonal indices could provide a more comprehensive understanding of arousal-behavior dynamics.

## RESOURCE AVAILABILITY

### Lead contact

Requests for further information and resources should be directed to and will be fulfilled by the lead contact, Liping Wang (lp.wang@siat.ac.cn).

### Materials availability

This study did not generate new reagents.

### Data and code availability

- All data reported in this paper will be shared by the lead contact upon request.
- The codes and software used in the study have been deposited at https://doi.org/10.5281/zenodo.15240963.
- Any additional information required to reanalyze the data reported in this paper is available from the lead contact upon request.

## ACKNOWLEDGMENTS

We thank Peng Cao for providing the FosTRAP2 mice line (Jackson Laboratory). We thank Yuwei Zhang and Qin Yang for the experimental help. This work was funded by the Strategic Priority Research Program of CAS (XDB1010301), the National Natural Science Foundation of China (32230042 to L.W. and 32371069 to X.L.), STI2030-Major Projects 2022ZD0211700, the Guangdong Province Basic Research Grant (2023B1515040009), the Shenzhen Science and Technology Program (KCXFZ20211020164543006 and JCYJ20210324102201003 to X.L.), the Financial Support for Outstanding Talents Training Fund in Shenzhen (L.W.), the Ten Thousand Talent Program, the Chang Jiang Scholars Program, the China Postdoctoral Science Foundation (2022M723299 and 2023T160666), the CAS Key Laboratory of Brain Connectome and Manipulation (2019DP173024), and the Guangdong Provincial Key Laboratory of Brain Connectome and Behavior (2023B1212060055). We sincerely thank the Shenzhen Brain Science Infrastructure for their essential technical support in this study.

## AUTHOR CONTRIBUTIONS

X.L. and L.W. designed the project. X.L., J.L., H.Z., Y.L., and X.Z. executed the experiments. X.L., C.H., H.Z., J.L., and K.H. analyzed the data. X.L., C.H., and L.W. wrote the manuscript. X.L., L.W., P.W., L.T., and F.X. revised the manuscript. X.L. and L.W. supervised the project.

## DECLARATION OF INTERESTS

L.W. serves on *Neuron*'s scientific advisory board.

## STAR★METHODS

Detailed methods are provided in the online version of this paper and include the following:

- KEY RESOURCES TABLE
- EXPERIMENTAL MODEL AND STUDY PARTICIPANT DETAILS
  - Male mice
- METHOD DETAILS
  - Viruses
  - Stereotaxic surgery
  - Anatomical tracing
  - Histology
  - c-Fos immunolabeling
  - Looming test
  - Pupillometry
  - Optogenetic manipulation
  - Fiber photometry
  - Behavioral analysis
  - *In vivo* extracellular recording
  - Spike sorting
  - Power spectrum analysis
- QUANTIFICATION AND STATISTICAL ANALYSIS

## SUPPLEMENTAL INFORMATION

Supplemental information can be found online at https://doi.org/10.1016/j.neuron.2025.04.018.

Received: September 6, 2024
Revised: February 28, 2025
Accepted: April 18, 2025
Published: May 9, 2025

## REFERENCES

1. Anderson, D.J., and Adolphs, R. (2014). A Framework for Studying Emotions across Species. Cell *157*, 187–200. https://doi.org/10.1016/j.cell.2014.03.003.
2. LeDoux, J. (2012). Rethinking the emotional brain. Neuron *73*, 653–676. https://doi.org/10.1016/j.neuron.2012.02.004.
3. Gross, C.T., and Canteras, N.S. (2012). The many paths to fear. Nat. Rev. Neurosci. *13*, 651–658. https://doi.org/10.1038/nrn3301.
4. Flavell, S.W., Gogolla, N., Lovett-Barron, M., and Zelikowsky, M. (2022). The emergence and influence of internal states. Neuron *110*, 2545–2570. https://doi.org/10.1016/j.neuron.2022.04.030.
5. Tseng, Y.-T., Schaefke, B., Wei, P., and Wang, L. (2023). Defensive responses: behaviour, the brain and the body. Nat. Rev. Neurosci. *24*, 655–671. https://doi.org/10.1038/s41583-023-00736-3.
6. Anderson, D.J. (2016). Circuit modules linking internal states and social behaviour in flies and mice. Nat. Rev. Neurosci. *17*, 692–704. https://doi.org/10.1038/nrn.2016.125.
7. McCormick, D.A., Nestvogel, D.B., and He, B.J. (2020). Neuromodulation of Brain State and Behavior. Annu. Rev. Neurosci. *43*, 391–415. https://doi.org/10.1146/annurev-neuro-100219-105424.
8. Hulsey, D., Zumwalt, K., Mazzucato, L., McCormick, D.A., and Jaramillo, S. (2024). Decision-making dynamics are predicted by arousal and uninstructed movements. Cell Rep. *43*, 113709. https://doi.org/10.1016/j.celrep.2024.113709.
9. Thompson, R.F., and Spencer, W.A. (1966). Habituation: A model phenomenon for the study of neuronal substrates of behavior. Psychol. Rev. *73*, 16–43. https://doi.org/10.1037/h0022681.
10. Steketee, J.D. (2016). The Neurobiology of Behavioral Sensitization. In Neurobiology of Addictions, A.C. Swann, F.G. Moeller, and M. Lijffijt,

eds. (Oxford University Press), pp. 138–152. https://doi.org/10.1093/med/9780199367894.003.0006.

11. Rankin, C.H., Abrams, T., Barry, R.J., Bhatnagar, S., Clayton, D.F., Colombo, J., Coppola, G., Geyer, M.A., Glanzman, D.L., Marsland, S., et al. (2009). Habituation revisited: An updated and revised description of the behavioral characteristics of habituation. Neurobiol. Learn. Mem. *92*, 135–138. https://doi.org/10.1016/j.nlm.2008.09.012.
12. Hattori, D., Aso, Y., Swartz, K.J., Rubin, G.M., Abbott, L.F., and Axel, R. (2017). Representations of Novelty and Familiarity in a Mushroom Body Compartment. Cell *169*, 956–969.e17. https://doi.org/10.1016/j.cell.2017.04.028.
13. Yilmaz, M., and Meister, M. (2013). Rapid Innate Defensive Responses of Mice to Looming Visual Stimuli. Curr. Biol. *23*, 2011–2015. https://doi.org/10.1016/j.cub.2013.08.015.
14. Wei, P., Liu, N., Zhang, Z., Liu, X., Tang, Y., He, X., Wu, B., Zhou, Z., Liu, Y., Li, J., et al. (2015). Processing of visually evoked innate fear by a non-canonical thalamic pathway. Nat. Commun. *6*, 6756. https://doi.org/10.1038/ncomms7756.
15. Shang, C., Chen, Z., Liu, A., Li, Y., Zhang, J., Qu, B., Yan, F., Zhang, Y., Liu, W., Liu, Z., et al. (2018). Divergent midbrain circuits orchestrate escape and freezing responses to looming stimuli in mice. Nat. Commun. *9*, 1232. https://doi.org/10.1038/s41467-018-03580-7.
16. Salay, L.D., Ishiko, N., and Huberman, A.D. (2018). A midline thalamic circuit determines reactions to visual threat. Nature *557*, 183–189. https://doi.org/10.1038/s41586-018-0078-2.
17. Evans, D.A., Stempel, A.V., Vale, R., Ruehle, S., Lefler, Y., and Branco, T. (2018). A synaptic threshold mechanism for computing escape decisions. Nature *558*, 590–594. https://doi.org/10.1038/s41586-018-0244-6.
18. Huang, L., Yuan, T., Tan, M., Xi, Y., Hu, Y., Tao, Q., Zhao, Z., Zheng, J., Han, Y., Xu, F., et al. (2017). A retinoraphe projection regulates serotonergic activity and looming-evoked defensive behaviour. Nat. Commun. *8*, 14908. https://doi.org/10.1038/ncomms14908.
19. Hayes, W.N., and Saiff, E.I. (1967). Visual alarm reactions in turtles. Anim. Behav. *15*, 102–106. https://doi.org/10.1016/S0003-3472(67)80018-6.
20. Matheson, T., Rogers, S.M., and Krapp, H.G. (2004). Plasticity in the Visual System Is Correlated With a Change in Lifestyle of Solitarious and Gregarious Locusts. J. Neurophysiol. *91*, 1–12. https://doi.org/10.1152/jn.00795.2003.
21. Oliva, D., Medan, V., and Tomsic, D. (2007). Escape behavior and neuronal responses to looming stimuli in the crab Chasmagnathus granulatus (Decapoda: Grapsidae). J. Exp. Biol. *210*, 865–880. https://doi.org/10.1242/jeb.02707.
22. Mancienne, T., Marquez-Legorreta, E., Wilde, M., Piber, M., Favre-Bulle, I., Vanwalleghem, G., and Scott, E.K. (2021). Contributions of Luminance and Motion to Visual Escape and Habituation in Larval Zebrafish. Front. Neural Circuits *15*, 748535. https://doi.org/10.3389/fncir.2021.748535.
23. Marquez-Legorreta, E., Constantin, L., Piber, M., Favre-Bulle, I.A., Taylor, M.A., Blevins, A.S., Giacomotto, J., Bassett, D.S., Vanwalleghem, G.C., and Scott, E.K. (2022). Brain-wide visual habituation networks in wild type and fmr1 zebrafish. Nat. Commun. *13*, 895. https://doi.org/10.1038/s41467-022-28299-4.
24. Zhao, X., Liu, M., and Cang, J. (2014). Visual Cortex Modulates the Magnitude but Not the Selectivity of Looming-Evoked Responses in the Superior Colliculus of Awake Mice. Neuron *84*, 202–213. https://doi.org/10.1016/j.neuron.2014.08.037.
25. Li, L., Feng, X., Zhou, Z., Zhang, H., Shi, Q., Lei, Z., Shen, P., Yang, Q., Zhao, B., Chen, S., et al. (2018). Stress Accelerates Defensive Responses to Looming in Mice and Involves a Locus Coeruleus-Superior Colliculus Projection. Curr. Biol. *28*, 859–871.e5. https://doi.org/10.1016/j.cub.2018.02.005.
26. Liu, X., Chen, C., Liu, Y., Wang, Z., Huang, K., Wang, F., and Wang, L. (2018). Gentle Handling Attenuates Innate Defensive Responses to Visual Threats. Front. Behav. Neurosci. *12*, 239. https://doi.org/10.3389/fnbeh.2018.00239.
27. Tseng, Y.T., Zhao, B., Chen, S., Ye, J., Liu, J., Liang, L., Ding, H., Schaefke, B., Yang, Q., Wang, L., et al. (2022). The subthalamic corticotropin-releasing hormone neurons mediate adaptive REM-sleep responses to threat. Neuron *110*, 1223–1239.e8. https://doi.org/10.1016/j.neuron.2021.12.033.
28. Liang, F., Xiong, X.R., Zingg, B., Ji, X.Y., Zhang, L.I., and Tao, H.W. (2015). Sensory Cortical Control of a Visually Induced Arrest Behavior via Corticotectal Projections. Neuron *86*, 755–767. https://doi.org/10.1016/j.neuron.2015.03.048.
29. Daviu, N., Füzesi, T., Rosenegger, D.G., Rasiah, N.P., Sterley, T.-L., Peringod, G., and Bains, J.S. (2020). Paraventricular nucleus CRH neurons encode stress controllability and regulate defensive behavior selection. Nat. Neurosci. *23*, 398–410. https://doi.org/10.1038/s41593-020-0591-0.
30. Li, C., Kühn, N.K., Alkislar, I., Sans-Dublanc, A., Zemmouri, F., Paesmans, S., Calzoni, A., Ooms, F., Reinhard, K., and Farrow, K. (2023). Pathway-specific inputs to the superior colliculus support flexible responses to visual threat. Sci. Adv. *9*, eade3874. https://doi.org/10.1126/sciadv.ade3874.
31. Yang, X., Liu, Q., Zhong, J., Song, R., Zhang, L., and Wang, L. (2020). A simple threat-detection strategy in mice. BMC Biol. *18*, 93. https://doi.org/10.1186/s12915-020-00825-0.
32. Redgrave, P., and Gurney, K. (2006). The short-latency dopamine signal: a role in discovering novel actions? Nat. Rev. Neurosci. *7*, 967–975. https://doi.org/10.1038/nrn2022.
33. Goldberg, M.E., and Wurtz, R.H. (1972). Activity of superior colliculus in behaving monkey. II. Effect of attention on neuronal responses. J. Neurophysiol. *35*, 560–574. https://doi.org/10.1152/jn.1972.35.4.560.
34. Ignashchenkova, A., Dicke, P.W., Haarmeier, T., and Thier, P. (2004). Neuron-specific contribution of the superior colliculus to overt and covert shifts of attention. Nat. Neurosci. *7*, 56–64. https://doi.org/10.1038/nn1169.
35. Krauzlis, R.J., Lovejoy, L.P., and Zénon, A. (2013). Superior Colliculus and Visual Spatial Attention. Annu. Rev. Neurosci. *36*, 165–182. https://doi.org/10.1146/annurev-neuro-062012-170249.
36. McFadyen, J., Dolan, R.J., and Garrido, M.I. (2020). The influence of subcortical shortcuts on disordered sensory and cognitive processing. Nat. Rev. Neurosci. *21*, 264–276. https://doi.org/10.1038/s41583-020-0287-1.
37. Bromberg-Martin, E.S., Matsumoto, M., and Hikosaka, O. (2010). Dopamine in Motivational Control: Rewarding, Aversive, and Alerting. Neuron *68*, 815–834. https://doi.org/10.1016/j.neuron.2010.11.022.
38. Brischoux, F., Chakraborty, S., Brierley, D.I., and Ungless, M.A. (2009). Phasic excitation of dopamine neurons in ventral VTA by noxious stimuli. Proc. Natl. Acad. Sci. USA *106*, 4894–4899. https://doi.org/10.1073/pnas.0811507106.
39. Lammel, S., Lim, B.K., Ran, C., Huang, K.W., Betley, M.J., Tye, K.M., Deisseroth, K., and Malenka, R.C. (2012). Input-specific control of reward and aversion in the ventral tegmental area. Nature *491*, 212–217. https://doi.org/10.1038/nature11527.
40. Zhou, Z., Liu, X., Chen, S., Zhang, Z., Liu, Y., Montardy, Q., Tang, Y., Wei, P., Liu, N., Li, L., et al. (2019). A VTA GABAergic Neural Circuit Mediates Visually Evoked Innate Defensive Responses. Neuron *103*, 473–488.e6. https://doi.org/10.1016/j.neuron.2019.05.027.
41. Barbano, M.F., Wang, H.L., Zhang, S., Miranda-Barrientos, J., Estrin, D.J., Figueroa-González, A., Liu, B., Barker, D.J., and Morales, M. (2020). VTA Glutamatergic Neurons Mediate Innate Defensive Behaviors. Neuron *107*, 368–382.e8. https://doi.org/10.1016/j.neuron.2020.04.024.
42. Sommer, M.A., and Wurtz, R.H. (2006). Influence of the thalamus on spatial visual processing in frontal cortex. Nature *444*, 374–377. https://doi.org/10.1038/nature05279.

43. Shin, A., Park, S., Shin, W., Woo, J., Jeong, M., Kim, J., and Kim, D. (2023). A brainstem-to-mediodorsal thalamic pathway mediates sound-induced arousal from slow-wave sleep. Curr. Biol. *33*, 875–885.e5. https://doi.org/10.1016/j.cub.2023.01.033.

44. Wolff, M., and Halassa, M.M. (2024). The mediodorsal thalamus in executive control. Neuron *112*, 893–908. https://doi.org/10.1016/j.neuron.2024.01.002.

45. Baek, J., Lee, S., Cho, T., Kim, S.-W., Kim, M., Yoon, Y., Kim, K.K., Byun, J., Kim, S.J., Jeong, J., et al. (2019). Neural circuits underlying a psychotherapeutic regimen for fear disorders. Nature *566*, 339–343. https://doi.org/10.1038/s41586-019-0931-y.

46. Craig, A.D.B. (2009). How do you feel–now? The anterior insula and human awareness. Nat. Rev. Neurosci. *10*, 59–70. https://doi.org/10.1038/nrn2555.

47. Underwood, E. (2021). A sense of self. Science *372*, 1142–1145. https://doi.org/10.1126/science.372.6547.1142.

48. Gogolla, N. (2017). The insular cortex. Curr. Biol. *27*, R580–R586. https://doi.org/10.1016/j.cub.2017.05.010.

49. Uddin, L.Q. (2015). Salience processing and insular cortical function and dysfunction. Nat. Rev. Neurosci. *16*, 55–61. https://doi.org/10.1038/nrn3857.

50. Deng, H., Xiao, X., Yang, T., Ritola, K., Hantman, A., Li, Y., Huang, Z.J., and Li, B. (2021). A genetically defined Insula-brainstem circuit selectively controls motivational vigor. Cell *184*, 6344–6360.e18. https://doi.org/10.1016/j.cell.2021.11.019.

51. Nicolas, C., Ju, A., Wu, Y., Eldirdiri, H., Delcasso, S., Couderc, Y., Fornari, C., Mitra, A., Supiot, L., Vérité, A., et al. (2023). Linking emotional valence and anxiety in a mouse insula-amygdala circuit. Nat. Commun. *14*, 5073. https://doi.org/10.1038/s41467-023-40517-1.

52. Gehrlach, D.A., Dolensek, N., Klein, A.S., Roy Chowdhury, R., Matthys, A., Junghänel, M., Gaitanos, T.N., Podgornik, A., Black, T.D., Reddy Vaka, N., et al. (2019). Aversive state processing in the posterior insular cortex. Nat. Neurosci. *22*, 1424–1437. https://doi.org/10.1038/s41593-019-0469-1.

53. Wang, Q., Zhu, J.-J., Wang, L., Kan, Y.-P., Liu, Y.-M., Wu, Y.-J., Gu, X., Yi, X., Lin, Z.-J., Wang, Q., et al. (2022). Insular cortical circuits as an executive gateway to decipher threat or extinction memory via distinct subcortical pathways. Nat. Commun. *13*, 5540. https://doi.org/10.1038/s41467-022-33241-9.

54. Aspide, R., Gironi Carnevale, U.A., Sergeant, J.A., and Sadile, A.G. (1998). Non-selective attention and nitric oxide in putative animal models of attention-deficit hyperactivity disorder. Behav. Brain Res. *95*, 123–133. https://doi.org/10.1016/S0166-4328(97)00217-9.

55. Aspide, R., Fresiello, A., de Filippis, G., Gironi Carnevale, U.A., and Sadile, A.G. (2000). Non-selective attention in a rat model of hyperactivity and attention deficit: subchronic methylphenydate and nitric oxide synthesis inhibitor treatment. Neurosci. Biobehav. Rev. *24*, 59–71. https://doi.org/10.1016/S0149-7634(99)00045-7.

56. Lawson, S.K., Gray, A.C., and Woehrle, N.S. (2016). Effects of oxytocin on serotonin 1B agonist-induced autism-like behavior in mice. Behav. Brain Res. *314*, 52–64. https://doi.org/10.1016/j.bbr.2016.07.027.

57. DeNardo, L.A., Liu, C.D., Allen, W.E., Adams, E.L., Friedmann, D., Fu, L., Guenthner, C.J., Tessier-Lavigne, M., and Luo, L. (2019). Temporal evolution of cortical ensembles promoting remote memory retrieval. Nat. Neurosci. *22*, 460–469. https://doi.org/10.1038/s41593-018-0318-7.

58. Shang, C., Liu, A., Li, D., Xie, Z., Chen, Z., Huang, M., Li, Y., Wang, Y., Shen, W.L., and Cao, P. (2019). A subcortical excitatory circuit for sensory-triggered predatory hunting in mice. Nat. Neurosci. *22*, 909–920. https://doi.org/10.1038/s41593-019-0405-4.

59. Zhang, X., and Li, B. (2018). Population coding of valence in the basolateral amygdala. Nat. Commun. *9*, 5195. https://doi.org/10.1038/s41467-018-07679-9.

60. Zingg, B., Chou, X.L., Zhang, Z.G., Mesik, L., Liang, F., Tao, H.W., and Zhang, L.I. (2017). AAV-Mediated Anterograde Transsynaptic Tagging: Mapping Corticocollicular Input-Defined Neural Pathways for Defense Behaviors. Neuron *93*, 33–47. https://doi.org/10.1016/j.neuron.2016.11.045.

61. Wang, L., Chen, I.Z., and Lin, D. (2015). Collateral Pathways from the Ventromedial Hypothalamus Mediate Defensive Behaviors. Neuron *85*, 1344–1358. https://doi.org/10.1016/j.neuron.2014.12.025.

62. Darwin, C. (1859). On the Origin of Species. Evolution and Creationism.

63. Abbey-Lee, R.N., and Dingemanse, N.J. (2019). Adaptive individual variation in phenological responses to perceived predation levels. Nat. Commun. *10*, 1601. https://doi.org/10.1038/s41467-019-09138-5.

64. Costa-Mattioli, M., and Walter, P. (2020). The integrated stress response: From mechanism to disease. Science *368*, eaat5314. https://doi.org/10.1126/science.aat5314.

65. Hoverman, J.T., and Searle, C.L. (2016). Behavioural influences on disease risk: implications for conservation and management. Anim. Behav. *120*, 263–271. https://doi.org/10.1016/j.anbehav.2016.05.013.

66. Fotowat, H., and Engert, F. (2023). Neural circuits underlying habituation of visually evoked escape behaviors in larval zebrafish. Elife *12*, e82916. https://doi.org/10.7554/eLife.82916.

67. Sprague, J.M. (1966). Interaction of Cortex and Superior Colliculus in Mediation of Visually Guided Behavior in the Cat. Science *153*, 1544–1547. https://doi.org/10.1126/science.153.3743.1544.

68. Zénon, A., and Krauzlis, R.J. (2012). Attention deficits without cortical neuronal deficits. Nature *489*, 434–437. https://doi.org/10.1038/nature11497.

69. Hu, F., and Dan, Y. (2022). An inferior-superior colliculus circuit controls auditory cue-directed visual spatial attention. Neuron *110*, 109–119.e3. https://doi.org/10.1016/j.neuron.2021.10.004.

70. Itti, L., and Koch, C. (2001). Computational modelling of visual attention. Nat. Rev. Neurosci. *2*, 194–203. https://doi.org/10.1038/35058500.

71. Peng, B., Huang, J.J., Li, Z., Zhang, L.I., and Tao, H.W. (2024). Cross-modal enhancement of defensive behavior via parabigemino-collicular projections. Curr. Biol. *34*, 3616–3631.e5. https://doi.org/10.1016/j.cub.2024.06.052.

72. Beckers, T., Hermans, D., Lange, I., Luyten, L., Scheveneels, S., and Vervliet, B. (2023). Understanding clinical fear and anxiety through the lens of human fear conditioning. Nat. Rev. Psychol. *2*, 233–245. https://doi.org/10.1038/s44159-023-00156-1.

73. Deisseroth, K. (2014). Circuit dynamics of adaptive and maladaptive behaviour. Nature *505*, 309–317. https://doi.org/10.1038/nature12982.

74. Kaiser, T., and Feng, G. (2015). Modeling psychiatric disorders for developing effective treatments. Nat. Med. *21*, 979–988. https://doi.org/10.1038/nm.3935.

75. Gururajan, A., Reif, A., Cryan, J.F., and Slattery, D.A. (2019). The future of rodent models in depression research. Nat. Rev. Neurosci. *20*, 686–701. https://doi.org/10.1038/s41583-019-0221-6.

## STAR★METHODS

### KEY RESOURCES TABLE

| REAGENT or RESOURCE | SOURCE | IDENTIFIER |
|---|---|---|
| Antibodies | | |
| Rabbit monoclonal anti-c-Fos | Cell Signaling | Cat#2250; RRID: AB_3696002 |
| Goat anti-rabbit alexa fluor@488-conjugated affinipure fab fragment | Jackson Immuno Research | Cat#111-547-003; RRID: AB_2338056 |
| Rabbit anti-Cre | Abcam | Cat#ab190177; RRID: AB_2860024 |
| Bacterial and virus strains | | |
| AAV2/9-CaMKIIα-ChR2-mCherry | Liping Wang's Lab at the CAS | N/A |
| AAV2/9-CaMKIIα-mCherry | Liping Wang's Lab at the CAS | N/A |
| AAV2/2Retro-hSyn-Cre-WPRE-pA | Taitool Bioscience Co., Ltd., Shanghai | N/A |
| AAV2/9-hSyn-jGCaMP7S-WPRE-pA | Taitool Bioscience Co., Ltd., Shanghai | N/A |
| AAV2/9-hSyn-DIO-jGCaMP7s-WPRE-PA | Taitool Bioscience Co., Ltd., Shanghai | N/A |
| AAV2/9-hSyn-DIO-hM4D(Gi)-eGFP-WPRE-pA | Taitool Bioscience Co., Ltd., Shanghai | N/A |
| AAV2/9-hSyn-DIO-stGtACR2-eGFP-WPRE-pA | Taitool Bioscience Co., Ltd., Shanghai | N/A |
| Rabies Virus- dG -dsRED | BrainCase Co., Ltd.,China | N/A |
| RV-dG-EGFP | BrainCase Co., Ltd.,China | N/A |
| AAV1-hSyn-SV40 NLS-Cre | BrainCase Co., Ltd.,China | N/A |
| Retro-AAV-hSyn-mCherry | BrainCase Co., Ltd.,China | N/A |
| Retro-AAV-hSyn-EYFP | BrainCase Co., Ltd.,China | N/A |
| AAV2/9-Ef1α-DIO-mCherry | Liping Wang's Lab at the CAS | N/A |
| AAV2/9-Ef1α-DIO-GFP | Liping Wang's Lab at the CAS | N/A |
| Deposited data | | |
| Computation code of in vivo recording | Zenodo | Zenodo: https://doi.org/10.5281/zenodo.15240963 |
| Chemicals, peptides, and recombinant proteins | | |
| DAPI | Thermofisher | Cat#62248 |
| Clozapine-N-Oxide | Apexbio | Cat# A3317 |
| Experimental models: Organisms/strains | | |
| C57BL/6J mice | Zhejiang Vital River Laboratory Animal Technology Co., Ltd., Zhejiang, China | N/A |
| FosTRAP2(Fos-2A-iCreER) | Jackson Laboratory | Stock No: 030323 |
| VGluT2-ires-Cre mice; Slc17a6tm2(cre)Lowl/J | The Jackson Laboratory | Stock No: 016963 |
| Software and algorithms | | |
| GraphPad Prism 9.0 | GraphPad Software Inc | http://www.graphpad.com/scientific-software/prism/ |
| MATLAB R2017a | The MathWorks, Inc. | https://ch.mathworks.com/products/matlab.html |
| Offline Sorter | Plexon Inc | https://plexon.com/products/offline-sorter/ |
| LabVIEW | National Instruments | https://www.ni.com/ |
| ImageJ | NIH | https://imagej.nih.gov/ij/ |
| Image Pro-plus | Media Cybernetics, Inc | http://en.freedownloadmanager.org/Windows-PC/Image-Pro-Plus.html |

(*Continued on next page*)

*Continued*

| REAGENT or RESOURCE | SOURCE | IDENTIFIER |
|---|---|---|
| Zen softwares | Zeiss | http://www.zeiss.com/corporate/en_de/global/home.html |
| Adobe Photoshop | Adobe Systems Inc | https://www.adobe.com/ |
| Adobe Premiere | Adobe Systems Inc | https://www.adobe.com/ |

## EXPERIMENTAL MODEL AND STUDY PARTICIPANT DETAILS

### Male mice

All experimental procedures were approved by the Animal Care and Use Committees at the Shenzhen Institute of Advanced Technology (SIAT), Chinese Academy of Sciences (CAS). Adult (6– 8 week-old) male C57BL/6J (Beijing Vital River Laboratory Animal Technology Co., Ltd., Beijing, China), VGLUT2-ires-Cre (#016963) and FosTRAP2 (#030323) mice were used in this study. Male mice were housed at 22–25°C on a circadian cycle of 12-h light and 12-h dark with ad-libitum access to food and water.

## METHOD DETAILS

### Viruses

For optogenetic experiments, we used plasmids for AAV2/9 viruses encoding *CaMKIIa*:: hChR2 (H134R)–mCherry, *CaMKIIa*:: mCherry, *EF1α*:: DIO–hChR2 (H134R)–mCherry, *EF1α*:: DIO–mCherry, *EF1α*:: DIO–EYFP and Retro-AAV-*EF1α*-DIO-hChR2 (H134R)–mCherry (packaged by BrainCase Co., Ltd., Shenzhen). AAV2/2Retro-hSyn-Cre-WPRE-pA, AAV2/9-hSyn-jGCaMP7S-WPRE-pA, AAV2/9-hSyn-DIO-jGCaMP7s-WPRE-PA, AAV2/9-hSyn-DIO-hM4D(Gi)-eGFP-WPRE-pA, AAV2/9-hSyn-DIO-stGtACR2-eGFP-WPRE-pA (packaged by Taitool Bioscience Co., Ltd., Shanghai). Viral vector titers were in the range of 3-6x$10^{12}$ genome copies per ml (gc)/mL. For viral tracing, viral vectors RV-dG-dsRed, RV-dG-GFP, Retro-AAV-hSyn-mCherry, Retro-AAV-hSyn-EYFP, AAV1-hSyn-SV40 NLS-Cre were used (packaged by BrainCase Co.). Adeno-associated and rabies viruses were purified and concentrated to titers at approximately $3\times10^{12}$ v.g/ml and $1\times10^{9}$ pfu/ml, respectively.

### Stereotaxic surgery

Animals were anesthetized with pentobarbital (i.p., 80 mg/kg) before stereotaxic injection. The viruses were injected into the SC (AP −3.80 mm, ML ±0.8 mm, and DV −1.8 mm), the Insula (AP +0.14 mm, ML ±3.75 mm, DV range between −3.75 and −3.9 mm), and the Cg (AP +0.3 mm, ML ±0.30 mm, DV −1.5 mm). Optical stimulation of terminals was conducted using a 200-μm optic fiber (NA: 0.37; NEWDOON, Hangzhou) unilaterally implanted into the VTA (AP −3.20 mm, ML −0.25 mm, DV −3.8 mm), MD (AP −1.3 mm, ML −0.30 mm, DV −3.2 mm), the SC (AP −3.80 mm, ML ±0.8 mm, DV −1.8 mm), and the BLA (AP −1.5 mm, ML ±3.1 mm, DV −4.70 mm). To block backpropagation of virus in SC, cannulas were implanted 0.3 mm above the SC (AP −3.80 mm, ML ±0.8 mm, DV −1.5 mm). Either bupivacaine (4%, 0.3 μl) or saline (control) was delivered into the SC 30 min before optogenetic modulation and behavioral tests. Mice had at least 2 weeks to recover after surgery before testing.

### Anatomical tracing

To investigate the origin of the SC-MD and SC-VTA or Insula-MD and Insula-VTA projecting neurons, we injected RV-dG-dsRed into the VTA and RV-dG-EGFP into the MD in the same animal. To demonstrate the different SC and Insula outputs, we injected AAV9-*EF1α*–mCherry into the SC and AAV9-*EF1α*–EYFP into the Insula. To map the axonal output of input-defined neurons in the VTA and MD, anterograde trans-synaptic AAV1-hSyn-SV40 NLS-Cre was unilaterally injected into the SC, *EF1α*:: DIO–mCherry was injected into the VTA and *EF1α*:: DIO–EYFP was injected into MD.

### Histology

Mice were given an overdose of pentobarbital and perfused with 0.9% saline followed by 4% paraformaldehyde (PFA) in PBS. Brains were dissected and postfixed in 4% PFA at 4°C for 24 h then transferred to 30% sucrose for 2 days. Coronal slices (40 μm) were taken across the entire rostrocaudal extent of the brain using a cryostat at −15°C and stored in 24-well plates containing cryoprotectant at 4°C. To visualize virus expression, optic fiber tips, optrode placements, and viral tracing targets, floating sections were blocked with 10% normal goat serum in PBS-T (0.03% Triton-X 100), and DAPI (1:50000, Cat#62248, Thermofisher). Brain sections were mounted and cover-slipped with Fluoromount aqueous mounting medium (Sigma-Aldrich, USA). Sections were then photographed using an Olympus VS120 virtual microscopy slide scanning system or a Zeiss LSM LSM 880 confocal microscope. Images were analyzed with ImageJ, Image Pro-plus, and Photoshop software.

Please cite this article in press as: Liu et al., Neural circuit underlying individual differences in visual escape habituation, Neuron (2025), https://doi.org/10.1016/j.neuron.2025.04.018





### c-Fos immunolabeling

To visualize c-Fos activity across the whole brain following optogenetic activation of specific neural circuits, we used different optogenetic stimulus groups: *CaMKIIa*::ChR2$_{Insula\text{-}BLA}$, *CaMKIIa*::mCherry$_{Insula\text{-}BLA}$ (control), and *CaMKIIa*::ChR2$_{Insula\text{-}MD}$ *CaMKIIa*::mCherry$_{Insula\text{-}MD}$ (control). Mice in each group were given 3 min habituation time and 2 presentations of optogenetic stimuli (20 Hz, 5 ms, 2.5 s, with an interval no less than 2 min) in a looming box during a 10–20 min session. Mice were sacrificed 1.5 hours following optogenetic activation and brains then stained for both c-Fos, Cre and DAPI. Sections were washed and incubated in primary (Rabbit anti-c-Fos,1:500, Cell Signaling, Cat#2250. CST; Rabbit anti-Cre, Abcam 1:1000, Cat# ab190177) and secondary (1:300, Cat#111-547-003, Jackson immuno research) antibodies and DAPI (1:50000, Cat#62248, Thermofisher). Imagines were taken using an Olympus VS120 virtual microscopy slide scanning system or a Zeiss LSM LSM 880 confocal microscope and then overlaid with The Mouse Brain in Stereotaxic Coordinates to locate brain nuclei. Then, c-Fos positive neurons were manually counted by an individual experimenter blind to the experiment groups using ImageJ and Photoshop software.

### Looming test

The looming test was performed in a closed Plexiglas box (40 x 40 x 30 cm) with a shelter nest in one corner. An LCD monitor was placed on the ceiling to present looming stimulus to the upper visual field. The stimulus was a black disc on a grey background expanding from a 2° to 20° visual angle, repeated 15 times, lasting a total of 5.5 s. Mouse behavior was recorded using a Sony FDR-AX45 camera. Mice were handled and habituated for 10 min to the looming box one day prior to the test. On the test day, mice were given 3 min to habituate to the box, then 10 looming stimulus trials were presented. The stimulus was triggered by the experimenter when the mouse was far from the shelter and the interval between each trial no less than 2 min. For optogenetic activation experiments with looming stimulus, mice received blue light (10 Hz, 473 nm; Aurora-220-473, NEWDOON, Hangzhou) at an intensity of 8 mW at the fiber tips. Light stimulation was delivered 1 s before onset of the looming stimulus and continued until the stimulus ended.

### Pupillometry

Mice were head-fixed and allowed to run freely on a stationary foam ball with a diameter of 20 cm during testing. Mice were first habituated to the ball for 3 consecutive days before recording began (day 1, 15 min; day 2, 30 min; day 3, 1 h). One eye of each mouse was illuminated with a 940 nm near-infrared light and the pupillary responses were recorded using a camera (Point Grey, FL3-U3-13E4M, set to 200 fps). Software (LabVIEW) was used to control the camera and process images in real time to obtain pupil data, including x position, y position, diameter of the pupil and the timestamp for each image. To avoid interference between pupil positions and pupil diameter accuracy, the ellipse long diameter was measured instead of the cross diameter and area.

Looming stimuli were presented using Matlab Psychtoolbox and displayed on a 19-inch screen (DELL, P1917S) during pupillometry recording. An area of 60 x 60 pixels in one corner of the screen light up during the test as a way of modulating brightness. Brightness changes were detected using a photodiode and these signals were transmitted to LabVIEW using the same circuit board and used to timestamp the stimuli time with the pupillary data.

### Optogenetic manipulation

A closed Plexiglas box (40 x 40 x 30 cm) with a shelter/nest in the corner was used for optogenetic stimulation experiments. Animals were handled and habituated to the looming box for 10 min one day prior to testing. During the looming test session, mice were allowed to freely explore the looming box for 3–5 min and then received either optogenetic manipulation or presentation of the looming stimuli. For optogenetic stimulation experiments, the implanted optic fibers were connected to a 473-nm blue light laser (Aurora-220-473, NEWDOON, Hangzhou) at approximately 15-20 mW for terminals stimulation. Optogenetic activation of neural circuits began 4–5 weeks after animals received stereotactic viral injections and fiber implants. During experiments, light was delivered to either Insula-BLA terminals, SC−VTA terminals, Insula-VTA terminals, SC−MD terminals or Insula-MD terminals. The light was delivered into the targeted regions simultaneously 1 s before onset of the looming stimulus and continued until 1 s after the end of the looming stimulus. Mice received 7.5 s blue light stimulation (150 laser pulses of 5 ms at 20 Hz) at axon terminals during pathway activation experiments. Three repeated light stimuli trials were delivered at about 3 min intervals via a manual trigger in the targeting regions and all light stimulation was manually presented by the experimenter. For all gain-of function experiments (optogenetic activation of ChR2), the activation was all unilateral. All loss-of-function experiments involving optogenetic stimulation of GtACR2 were performed bilaterally.

### Fiber photometry

To monitor the neuronal calcium dynamics in VTA and MD, C57BL/6J mice were unilaterally injected with AAV2/9-hSyn-jGCaMP7S-WPRE-pA into the VTA and MD. For specific monitoring of calcium activity in SC→VTA and SC→MD or Insula→VTA and Insula→MD projecting neurons, C57BL/6J mice were unilaterally injected with AAV2/9-hSyn-DIO-jGCaMP7S-WPRE-pA into the SC or Insula, with concurrent retrograde targeting through ipsilateral VTA/MD injections of AAV2/2-Retro-hSyn-Cre-WPRE-pA. Three weeks post-injection, optical fibers were implanted into the VTA and MD at the same cerebral hemisphere of virus injection. Fibers were secured to the skull using screws and dental cement. Mice had at least 2 weeks to recover after surgery before testing.One day before the test day, the mice were acclimated to the fiber for at least 15 min in the looming box. On the test day, mice were given 3 min to habituate to the box, followed by 10 looming stimulus trials in a 3-min interval. Neural activity was recorded using a fiber

photometry system (Thinker Tech Bioscience Co., Nanjing, China) at 50 Hz, synchronized with a digital video capture for behavioral quantification. The excitation power at 470 nm was restricted to 20-40 μW at the fiber tip to minimize fluorescence bleaching.

Raw calcium fluorescence signals were processed using MATLAB (MathWorks, Natick, MA, USA). The values of fluorescence change (ΔF/F) were calculated as (F-F0)/(F0-Voffset), where F0 is the baseline fluorescence signal averaged over a 2 s time-window prior to the looming stimulus and Voffset is the fluorescence signal recorded before the cannula was connected to the optical fiber. ΔF/F values are presented as average plots with a shaded area indicating the SEM. The curve is smoothed using a 25-sample symmetric moving average filter. For quantitative analysis, area under curve (AUC) of ΔF/F values during the 5.5-s stimulus epochs (from the onset to the offset of looming stimulus) was calculated using the average plots.

### Behavioral analysis

Behavioral data were analyzed using Adobe Premiere software and observers were blind to experimental conditions. Mice were allowed to move freely in the open field with a shelter/nest before looming stimulus or light stimulation. Individual time courses were represented setting T=0 ms as the time of stimulation. Three parameters extracted from the behavioral experiments were used to quantify the looming-evoked or light-evoked defensive behavior: (1) rearing frequency: frequency of rearing on hindlimbs and leaning against the walls with one or both forepaws were visually monitored in 1-min blocks. (2) response latency: time between the onset of the looming stimulus or photostimulation and the onset of the escape, escape was defined as the motion that resulted in shelter entrance within stimulation period. (2) return time: the time from looming stimulus or photostimulation presentation to time when the mouse entered the nest. (3) Duration in nest: time spent in the nest following looming stimulus or photostimulation. Data obtained from mice with imprecise fiber placements were not used for analyses.

### *In vivo* extracellular recording

Mice were habituated to the head-fixed position to a magnet whilst on a foam ball 1 h each day for 3 days. Then, using a 16-channel micro-electrode (Neuronexus, A4x4-6mm-100-125-177-A16) and a multi-channel recording system (OmniPlex D, Plexon, Dallas, USA), the target brain regions were recorded. Electrodes were connected to a headstage (Plexon, Dallas, USA) containing 16-32 unity-gain operational amplifiers. The headstage was connected to a 16-channel computer-controlled preamplifier (gain X-100, band-pass fifilter from 150 Hz to 40 kHz, Plexon). Neuronal activity was digitized at 40 kHz and band-pass filtered from 300 Hz to 8 kHz, and isolated by time-amplitude window discrimination and template matching using a Multichannel Acquisition Processor system (Plexon). To investigate optogenetic effects, we inserted an optic fiber (200 μm diameter; 0.22 NA) 50 μm above the stimulated brain region. Before optical stimulation, we recorded for approximately 3 min to establish a stable electrode position inside the brain tissue. When the signal in the BLA was stable, optical stimulation was delivered at 1 min intervals. At least 10 repetitions of light stimulation was recorded during each session. At the conclusion of the experiment, recording sites were marked with DiI cell labeling solution (Invitrogen, USA) before perfusion, and electrode locations were reconstructed using standard histological techniques. Then, using a 16-channel micro-electrode (Neuronexus, A4x4-6mm-100-125-177-A16) and a multi-channel recording system (OmniPlex D, Plexon, Dallas, USA), the target brain regions were recorded. Electrodes were connected to a headstage (Plexon, Dallas, USA) containing 16-32 unity-gain operational amplifiers. The headstage was connected to a 16-channel computer-controlled preamplifier (gain X-100, band-pass fifilter from 150 Hz to 40 kHz, Plexon). Neuronal activity was digitized at 40 kHz and band-pass filtered from 300 Hz to 8 kHz, and isolated by time-amplitude window discrimination and template matching using a Multichannel Acquisition Processor system (Plexon). To investigate optogenetic effects, we inserted an optic fiber (200 μm diameter; 0.22 NA) 50 μm above the stimulated brain region. Before optical stimulation, we recorded for approximately 3 min to establish a stable electrode position inside the brain tissue. When the signal in the BLA was stable, optical stimulation was delivered at 1 min intervals. At least 10 repetitions of light stimulation were recorded during each session. At the conclusion of the experiment, recording sites were marked with DiI cell labeling solution (Invitrogen, USA) before perfusion, and electrode locations were reconstructed using standard histological techniques.

### Spike sorting

Single-unit spike sorting was performed using Plexon Offline Sorter software (Plexon, Inc., Dallas, TX, USA), then analyzed in Neuroexplorer (Nex Technologies, Madison, AL, USA) and Matlab (MathWorks, Natick, MA, USA). Principal-component scores were calculated for unsorted waveforms and plotted in a three-dimensional principal-component space; clusters containing similar valid waveforms were manually defined. A group of waveforms was considered to be generated from a single neuron if it defined a discrete cluster in principal component space that was distinct from clusters for other units and if it displayed a clear refractory period (>1 ms) in the auto-correlogram histograms. To avoid analysis of the same neuron recorded on different channels, we computed cross-correlation histograms. If a target neuron presented a peak of activity at a time that the reference neuron fired, only one of the two neurons was considered for further analysis.

To determine whether the firing rate of a particular BLA neuron was altered in response to optogenetic activation of the Insula (or SC-VTA, SC-MD, Insula, Insula-MD) axon terminals, we used peristimulus time histograms (PSTHs) to analyze firing pattern (Buzsaki et al., 2004). We calculated PSTHs using a 7.5 s period before and after onset of optogenetic stimulus with a bin size of 100 ms. We calculated the basal spontaneous firing rate of each neuron by averaging the PSTH over the pre-stimulus bins. Peak optogenetically-evoked firing rate was then calculated as the maximum value of the PSTH after stimulus onset (within 2.5 s from the stimulus). The

Please cite this article in press as: Liu et al., Neural circuit underlying individual differences in visual escape habituation, Neuron (2025), https://doi.org/10.1016/j.neuron.2025.04.018





baseline mean was the average of the PSTH bins before stimulus onset, and the SD was the standard deviation of the PSTH bins before stimulus onset. We calculated a *Z* score firing rate using the following equation: Z = (FR − mean of FRb)/SD of FRb, where FR indicates the firing rate for each bin and FRb indicates the baseline firing rate before the stimulus onset. A positive responding neuron was defined when the absolute value of the *Z* score firing rate of least one time bin after stimulation was larger than 2. Negative responding neurons were defined when the absolute value of the *Z* score firing rate of least one time bin after stimulation was smaller than -2.

### Power spectrum analysis

The LFP data before and after optogenetic stimulation was conducted with power spectrum analysis, which is a technique for decomposing complex signals into simpler signals based on Fourier transform. The power spectral density (PSD) for LFP data was computed using the multi-taper method (TW = 3, K = 5 tapers) using the Chronux toolbox using custom-written or existing functions in MATLAB (The Math Works).

## QUANTIFICATION AND STATISTICAL ANALYSIS

All looming behavioral videos were analyzed frame by frame manually using Adobe Premiere. In vivo multichannel recording data acquisition and analysis were conducted using Plexon and MATLAB, respectively. All the experimenters and analysts were different individuals, and the process was double-blinded. Data distribution was assumed to be normal, but this was not formally tested. Data were processed and analyzed using Graph Pad Prism 9 (GraphPad Software, Inc.), MATLAB, offline sorter, LabVIEW and image J, Image Pro-Plus, Zen softwares, Adobe photoshop, Adobe Premiere. All results are expressed as mean ± SEM. Data of non-paired samples were analyzed with two-tailed non-parametric Mann-Whitney U test, paired Student's t test, unpaired Student's t test, one-way ANOVA and two-way ANOVA were used where appropriate. Bonferroni post-hoc comparisons were conducted to detect significant main effects or interactions. Post-hoc significance values were set at $^{*}p < 0.05$, $^{**}p < 0.01$, $^{***}p < 0.001$ and $^{****}p < 0.0001$.

Details are available in Table S1.